Pergamon

0045-7949(95)00264-2

Computers & Structures Vol. 59, No. 3, pp. 489–527, 1996

0045-7949/96 $15.00 + 0.00

APPROXIMATE METHOD FOR THE OPTIMUM DESIGN OF RING AND STRINGER STIFFENED CYLINDRICAL PANELS AND SHELLS WITH LOCAL, INTER-RING, AND GENERAL BUCKLING MODAL IMPERFECTIONS

D. Bushnell and **W. D. Bushnell**

Department 93-30, 255, Lockheed Palo Alto Research Laboratory, 3251 Hanover St, Palo Alto, CA 94394, U.S.A.

(*Received* 30 *September* 1994)

Abstract—The PANDA2 computer program for minimum-weight design of stiffened composite panels is expanded to handle optimization of ring and stringer stiffened cylindrical panels and shells with three types of initial imperfections in the form of buckling modes, any combination of which may be present: local (buckling between adjacent stringers and rings), inter-ring (buckling between rings with stringers bending with the panel skin), and general (buckling in which both stringers and rings bend with the panel skin). Stresses and buckling load factors of the imperfect panels are computed with use of the assumption that the amplitudes of the buckling modal imperfections grow hyperbolically with increasing load factor according to the formula $AMP(i) = EIG(i)/(EIG(i) - 1)$, in which $AMP(i)$ is a factor to be multiplied by the initial buckling modal imperfection and $EIG(i)$ represents the critical load factor for the ith type of buckling mode ($i = 1$ = local buckling, $i = 2$ = inter-ring buckling, $i = 3$ = general buckling). Buckling load factors corresponding to local, inter-ring, and general buckling of the imperfect panel are computed with use of the maximum radius of curvature that develops in whatever portion of the panel (between stiffeners, inter-ring, overall) is being considered in the calculations and including redistribution of stress resultants over panel skin and stiffener cross-sections caused by prebuckling bending. Stress constraints in the optimization problem are computed including local, inter-ring, and general bending stresses generated by the growth of the initial local, inter-ring, and general imperfections. These bending stresses are added to the stresses from other sources (thermal, in-plane loading, normal pressure, curing, redistribution of membrane stresses from overall prebuckling bending of the imperfect panel). Minimum-weight designs for various imperfect unstiffened and stiffened cylindrical shells derived by PANDA2 are evaluated with use of the STAGS general-purpose finite element code. The agreement of results from PANDA2 and STAGS appears to qualify PANDA2 for the preliminary design of imperfect, stiffened, composite cylindrical shells.

INTRODUCTION

Previous work done

There is extensive literature on the buckling and postbuckling behavior of stiffened plates and shells. This literature covers metallic panels and panels fabricated from laminated composite materials. A brief survey of previous work in this field is given by Bushnell and Bushnell [1]. That survey will not be repeated here.

There have recently appeared many new papers on the buckling and postbuckling behavior of panels and on optimization of composite panels. New methods for the optimization of laminated composite panels have been explored by Haftka and his colleagues [2–5]. Preliminary feasibility and design studies of hypersonic aerospace planes have stimulated research on thermal buckling and postbuckling [6–11]. The relatively large effect of transverse shear deformation on the buckling and postbuckling behavior of laminated composite and sandwich panels is studied in several new papers [12–18]. Other new papers on the buckling and postbuckling of laminated composite panels and shells include Refs [19–29]. Of particular interest is a paper by Arbocz and Hol [30] on the development and linking of a suite of programs of increasing complexity operated on workstations at the Delft University of Technology.

Bushnell and Bushnell [1, 31] present the results of optimization of metallic and laminated composite Tee-stiffened and Hat-stiffened panels by the PANDA2 program [1, 32–37] and verification of the optimum design by the STAGS program [39–41, 48–50].

Purpose of this paper

The purpose of this paper is to describe extensions to the PANDA2 program that permit the optimum design of imperfect, stiffened cylindrical panels and shells as summarized in the abstract and to present

examples. The unique and most significant aspects of the work are felt to be:

(1) the generation of a reasonably user-friendly and practical computer program for the quick preliminary design of stiffened composite panels that may be imperfect, subject to multiple combinations of loads, and in which the panel skin may be in its locally postbuckled state, and

(2) the verification of this program through evaluation of optimum designs generated by it with use of the widely used general purpose code for nonlinear shell analysis, STAGS.

Scope of PANDA2

PANDA2 finds minimum weight designs of laminated composite flat or curved cylindrical panels or cylindrical shells with stiffeners in one or two orthogonal directions. Stiffeners can be blades, tees, angles, or hats. Truss-core sandwich panels and isogrid panels can also be handled. The panels or shells can be loaded by as many as five combinations of in-plane loads, edge moments, normal pressure, and temperature. Transverse shear deformation effects are included. The material properties can be temperature-dependent. Panels can be optimized for service in their locally postbuckled states. The presence of an overall imperfection, an inter-ring imperfection, and a local imperfection in the form of the general, inter-ring, and local buckling modes are included. Constraints on the design include stiffener crippling, local and general buckling, torsion-bending buckling of stringers and panel skin, stiffener "popoff", maximum displacement under pressure, maximum tensile or compressive stress along the fibers and normal to the fibers in each lamina, and maximum in-plane shear stress in each lamina. In calculating local buckling and postbuckling behavior, PANDA2 uses a single panel module which consists of one stringer plus the stringer base and panel skin on either side of it that represents the stringer spacing b. The cross-section of the panel module is discretized, and variation of behavior in the axial direction (parallel to the stringers) is represented by trigonometric functions. Optimization is performed with use of the ADS program developed by Vanderplaats and Sugimoto [42]. Further details about PANDA2 are provided in Refs [1, 31–37].

INTRODUCTION OF BUCKLING MODAL IMPERFECTIONS

Overview

Previously in PANDA2, global and local initial geometric imperfections affected buckling load factors and post-local-buckling behavior only in the following rather indirect ways:

(a) a global imperfection, or panel bowing, affected the distribution of resultants over the various segments of a panel module only for a flat panel or for a cylindrical panel without rings;

(b) a local imperfection affected the local postbuckling behavior and influenced the optimum design only for discretized models used in certain analysis branches. Local imperfections could not be used with panels or shells stiffened by rings only.

These influences of initial imperfections are still included, of course. However, they do not account in a strong enough way for the effect of initial geometric imperfections on the general, inter-ring, and local buckling load factors of stiffened cylindrical (in contrast to flat) panels, nor on the effect on maximum stress of imperfect cylindrical panels analyzed via the simple PANDA [34] type of analysis, nor on all of the effects on local buckling of stiffener parts caused by redistribution of stress resultants over these parts generated from the prebuckling bending that arises from the presence of inter-ring and general initial imperfections.

In the case of cylindrical panels (in contrast to flat panels), two new imperfection types, ovalization and inter-ring, have been introduced in PANDA2. There now exist in PANDA2 four types of imperfections: (1) local buckling modal; (2) inter-ring buckling modal; (3) general buckling modal; plus (4) overall uniform ovalization. The three buckling modal imperfections are assumed to have the forms of the critical local, inter-ring, and general buckling modes predicted from the closed form PANDA type of analysis [34]. For discretized models the local buckling mode is that predicted from the discretized single skin-stringer panel module, as described in previous papers on PANDA2. There does not yet exist in PANDA2 any discretized single skin-RING panel module model.

If the panel is flat the overall imperfection is assumed to be in the form of axial bowing.

Table 1 is a list of the section of the PANDA2 input data prompting file (called PROMPT.DAT) that is associated with input from the user pertaining to the various types of imperfections now permitted in the PANDA2 model. In order to obtain optimum designs of imperfect panels and shells, the user must be prepared to supply amplitudes for the various types of imperfections that reflect reasonably well the quality of the panel he or she eventually plans to fabricate.

If the panel is cylindrical the four types of imperfections affect buckling load factors calculated via PANDA-type (closed form, Bushnell [34]) models in a direct way: through modification of the effective radius of the entire panel or panel segment. In addition, the imperfections affect the buckling load factors in the somewhat indirect ways (a) and (b) listed at the beginning of this section. New knockdown factors are calculated in PANDA2 for general instability (skin, stringers, and rings all buckle together), inter-ring buckling (skin and

stringers buckle between rings), and local buckling (skin buckles between adjacent stringers and rings). These new knockdown factors are calculated by means of PANDA-type buckling analyses [34] conducted for both perfect and imperfect cylindrical panels in which the effect of each imperfection type (local, inter-ring, general, and ovalization) is to reduce the curvature of that portion of the panel included in the models for local, inter-ring, and general buckling, thereby reducing the buckling load factor governing that portion of the panel. The influence of amplification of each initial imperfection component during loading on the effective curvature of the imperfect panel is accounted for, both for stress and buckling analyses. In computations of the effective radius of curvature for local buckling, the combined influences of the general, inter-ring, and local imperfection components are accounted for.

The knockdown factors are the ratios,

$$\text{Knockdown factors, } K(i) = \text{EIG(imperfect, } i)/\text{EIG(perfect, } i) \quad (1)$$

in which EIG(*, i) are the critical buckling load factors computed from the closed form PANDA-type of analysis for $i = 1$ (local), $i = 2$ (inter-ring), and $i = 3$ (general) buckling for the imperfect (with initial imperfection suitably amplified by the applied loads) and the perfect configurations.

The imperfections also give rise to additional bending and twisting stresses when the imperfect panel is loaded. These additional stresses are now accounted for in the calculation of the stress constraints.

The effect of redistribution of stress resultants over the various stiffener parts during prebuckling bending of the imperfect cylindrical panel is also accounted for. Buckling load factors for the webs of stringers and rings are computed including the effect of linear variation of compression over the ring and stringer web cross-sections from the panel skin to the outstanding flanges.

Form of each of the buckling modal imperfections

This section holds for each type of buckling modal imperfection (local, inter-ring, general).

If the panel or section of the panel being considered in the current general, inter-ring or local buckling analysis is "long" in the x-direction (x = axial coord., see Fig. 9 of Ref. [34]), the shape of the buckling modal imperfection is assumed to have the form

$$\text{wimp}(x, y) = wo * \sin(ny) * \sin[m(x - cy)]. \quad (2)$$

If the panel or section of panel is "long" in the y-direction (y = circumferential coordinate), the shape of the buckling modal imperfection is assumed to have the form

$$\text{wimp}(x, y) = wo * \sin[n(y - \text{d}x)] * \sin(mx). \quad (3)$$

The variables n and m are given by

$$n = N*pi/B \quad m = M*pi/A, \quad (4)$$

where M and N are the number of halfwaves over the lengths A and B, respectively, and A and B are the circumferential and axial lengths of whatever portion of the entire panel is being considered: for local buckling the portion between adjacent stringers and rings; for inter-ring buckling the portion between adjacent rings; and for general buckling the entire panel.

These modes are shown in Fig. 9 of Ref. [34]. The variables n and m are defined in eqn (52) of Ref. [34], and c and d are the slopes of nodal lines of the buckling modes shown in Fig. 9 of Ref. [34]. Either c or d is always zero.

Equations (2) and (3) lead to the following curvature changes in twist:

For panels or sections of panel that are "long" in the x-direction ($d = 0$; c not equal 0):

$$\begin{aligned} w,xx(\text{imp}) &= wo*m**2* \sin(ny)* \sin[m(x - cy)] \\ w,yy(\text{imp}) &= wo*\{(n**2 + m**2*c**2)* \\ &\quad \sin(ny)* \sin[m(x - cy)] \\ &\quad + 2*n*m*c* \cos(ny)* \cos[m(x - cy)]\} \\ w,xy(\text{imp}) &= wo*\{m*n* \cos(ny)* \cos[m(x - cy)] \\ &\quad + m**2*c* \sin(ny)* \sin[m(x - cy)]\}. \end{aligned} \quad (5)$$

For panels or sections of panel that are "long" in the y-direction ($c = 0$; d not equal 0):

$$\begin{aligned} w,xx(\text{imp}) &= wo*\{(m**2 + n**2*d**2)* \\ &\quad \sin(mx)* \sin[n(y - \text{d}x)] \\ &\quad + 2*m*n*d* \cos(mx)* \\ &\quad \cos[n(y - \text{d}x)]\} \\ w,yy(\text{imp}) &= wo*n**2* \sin(mx)* \sin[n(y - \text{d}x)] \\ w,xy(\text{imp}) &= wo*\{m*n* \cos(mx)* \cos[n(y - \text{d}x)] \\ &\quad + n**2*d* \sin(mx)* \sin[n(y - \text{d}x]\}. \end{aligned} \quad (6)$$

Table 1. The part of the PANDA2 PROMPT.DAT file concerned with initial imperfections

343.0

Your panel is FLAT (not CYLINDRICAL). Therefore you will next be asked to provide amplitudes for the following modes of initial geometric imperfections (Wimpg, Wloc):

(a) initial overall bowing imperfection amplitude, Wimpg

NOTE: If the panel is stiffened, the sign of the initial overall bowing imperfection Wimpg is important because it affects how the panel skin and stiffener cross-sections of the initially bent panel become loaded under the applied loads. Type H(elp) for a discussion of this when you are prompted for Wimpg.

(b) local buckling modal imperfection amplitude, Wloc

The sign of Wloc is NOT significant. The local imperfection is assumed to have the same shape as the local buckling mode of the panel.

344.0

Your panel is CYLINDRICAL (not FLAT). Therefore you will next be asked to provide amplitudes for the following modes of initial geometric imperfection (Wimpg1, Wimpg2, Wpan, Wloc):

(a) overall out-of-roundness amplitude, Wimpg1, where
Wimpg1 = (Max. diameter–Min. diameter)/4.
NOTE: Whatever circumferential angle the panel spans, pretend for the purpose of this input datum that it represents part of a complete (360°) cylindrical shell that has an out-of-roundness with amplitude Wimpg1. If Wimpg2 (see next paragraph) is zero, the sign of Wimpg1 is significant. Otherwise, Wimpg1 will have the same sign as Wimpg2 in the calculations in PANDA2.

(b) overall buckling modal imperfection amplitude, Wimpg2.
NOTE: If the panel is stiffened, the sign of the overall buckling modal imperfection Wimpg2 is important because it affects how the panel skin and stiffener cross sections of the imperfect panel become loaded under the applied loads. Type H(elp) for a discussion of this when you are prompted for Wimpg2.

(c) if there are rings, inter-ring buckling modal imperfection amplitude, Wpan. NOTE: The sign of Wpan is important for the same reason given in Paragraph (b).

(d) local buckling modal imperfection amplitude, Wloc.
The sign of Wloc is NOT significant.

345.1 Initial bowing imperfection ampltiude (type H for sign), Wimpg
345.2

Positive Wimpg is downward in Fig. 9 of the long 1987 PANDA2 paper. The imperfection varies as sin $(pi*x/L)$ in the axial coordinate direction. A positive Wimpg causes the bottom skin surface to be convex. (The bottom surface is the surface of the skin opposite to that to which the stringers are attached). There is no prestress, either membrane or bending, associated with this bowing imperfection. It is hard to make a general statement whether positive or negative Wimpg will lead to earlier failure: Positive Wimpg combined with axial compression tends to cause greater compressive loads in the stringer web and flange and therefore tends to cause earlier buckling and rolling of these parts of the structure; Negative Wimpg combined with axial compression tends to cause greater compression in the panel skin and therefore earlier local buckling and higher local bending stresses in the postbuckling regime. It may be a good idea to set up two load cases, both with the same mechanical loads, the first with a positive Wimpg and the second with a negative Wimpg. Then the optimized design will be good no matter what the sign of the bowing imperfection Wimpg is.

If in doubt, use a NEGATIVE bowing imperfection (panel skin compressed more than stringer tips).

Continued opposite

Table 1—*continued*

346.1 Do you want to change WIMPG to a negative value?
346.2

If this set of applied loads is associated with only one value of bowing imperfection WIMPG, then it is generally best to use a negative value.

347.1 Initial local imperfection amplitude (must be positive), Wloc
347.2

In PANDA2 the local imperfection is assumed to have the same shape as the local buckling mode. Use a positive number for the amplitude, Wloc.

If you set Wloc = 0.0, PANDA2 will automatically reset Wloc to a value equal to ten percent of the thickness of the panel skin midway between stringers. This is a rather large initial imperfection. If you want to analyze a perfect panel, please provide a very small, but nonzero and positive, Wloc.

348.1 Out-of-roundness, Wimpg1 = (Max. diameter–Min. diam)/4, Wimpg1
348.2

The initial overall out-of-roundness amplitude is given by:
Wimpg1 = (Max. diameter–Min. diameter)/4.

NOTE: Whatever circumferential angle the panel spans, pretend for the purpose of this input datum that the panel represents part of a complete (360°) cylindrical shell that has an out-of-roundness with amplitude Wimpg1 = (Max. diameter–Min. diameter)/4.

349.1 Initial buckling modal general imperfection amplitude, Wimpg2
349.2

In PANDA2 the general imperfection is assumed to have the same shape as the general buckling mode obtained from a PANDA-type (closed form) analysis of the cylindrical panel.

IMPORTANT NOTE:
If the panel has axial stiffeners (stringers) and no rings and if the analysis mode IQUICK = 0, then:
You should consider optimizing with both negative and positive Wimpg2. Under axial loading, negative Wimpg2 gives rise to more compression in the skin than in the tips of the stringers. The opposite is true for positive Wimpg2. You can optimize for both positive and negative Wimpg2 by introduction of two load cases in MAINSETUP with everything the same in each except the sign of Wimpg2.
With IQUICK = 1, optimization with both positive and negative Wimpg2 is automatically performed within a single load case.

350.1 Initial buckling modal inter-ring imperfection amplitude, Wpan
350.2

This imperfection is used only if the panel is curved and there are both stringers and rings in the PANDA2 model. (See ITEM 124. in PANDA2.NEWS). In PANDA2 the inter-ring imperfection is assumed to have the same shape as the inter-ring buckling mode.

IMPORTANT NOTE: If IQUICK = 0, then:
You should consider optimizing with both negative and positive Wpan. Under axial loading, negative Wpan gives rise to more compression in the skin than in the tips of the stringers. The opposite is true for positive Wpan. You can optimize for both positive and negative Wpan by introduction of two load cases in MAINSETUP with everything and same in each except the sign of Wpan.
With IQUICK = 1, optimization with both positive and negative Wpan is automatically performed within a single load case.

351.1 Initial local imperfection amplitude (must be positive), Wloc
351.2

In PANDA2 the local imperfection is assumed to have the same shape as the local buckling mode. Use a positive number for the amplitude, Wloc.

If you set Wloc = 0.0, PANDA2 will automatically reset Wloc to a value equal to ten percent of the thickness of the panel skin midway between stringers. This is a rather large initial imperfection. If you want to analyze a perfect panel, please provide a very small, but nonzero and positive, Wloc.

Bending, twisting strains and amplification of the imperfection

Equations (5) and (6) are used to calculate bending and twisting stresses in cylindrical panels. If it is assumed that the initial imperfection grows hyperbolically, the additional bending and twisting strains at the applied load are given by:

$$\text{additional bending strains} = (+ \text{ or } -)(z*w,xx(\text{imp}) \text{ or } z*w,yy(\text{imp}))*[1/(\text{lambda}-1)] \quad (7)$$

$$\text{additional twisting strains} = (+ \text{ or } -)(2z*w,xy(\text{imp}))*[1/(\text{lambda}-1)] \quad (8)$$

in which the quantity z is the distance from a reference surface measured normal to that surface, and lambda, a buckling load factor, is obtained by iteration.

The additional bending and twisting strains are computed corresponding to local, inter-ring, and general buckling modal imperfections. They are added to the strains from other sources to compute the total strains and stresses throughout the panel and stiffener parts.

Nonhyperbolic growth of local imperfection

In many cases the assumption of hyperbolic growth of the LOCAL imperfection amplitude with load [growth proportional to the factor 1/(lambda − 1) shown in eqns (7), (8)] is too conservative. For example, in an axially compressed stringer-stiffened panel, the amplitude of the local imperfection grows more slowly than with 1/(lambda − 1) for loads near and above the critical local buckling load because the stringers absorb a larger and larger percentage of the total applied load as the panel skin bends between adjacent stringers.

An algorithm has been introduced into PANDA2 that is entered only if there is at least one set of stiffeners and if there is only one halfwave in the local buckling mode in at least one of the coordinate directions. The algorithm is based on the assumption that the panel skin is inextensional. Therefore, all of the applied membrane strain (for example, end shortening in the case of an axially compressed axially stiffened cylindrical panel) is assumed to be "absorbed" in the panel skin by out-of-plane rotation, dw/dx and dw/dy $(w,x; w,y)$. Whereas the extensional strain-displacement relations of the locally imperfect panel are given by:

$$ex = u,x + w,x(0)*w,x + 0.5*(w,x)**2$$

$$ey = v,y + w/r + w,y(0)*w,y + 0.5*(w,y)**2$$

$$exy = v,x + u,y + w,x(0)*w,y + w,y(0)*w,x + w,x*w,y \quad (9)$$

it is assumed [ONLY for the purpose of calculating the alternative amplification factor which is less conservative than 1/(lambda − 1)!] that

$$ex = w,x(0)*w,x + 0.5*(w,x)**2$$

$$ey = w,y(0)*w,y + 0.5*(w,y)**2$$

$$exy = w,x(0)*w,y + w,y(0)*w,x + w,x*w,y. \quad (10)$$

Furthermore, the local strain components, ex, ey, exy, are identified with (set equal to) the average applied in-plane strain components ETOT1, ETOT2, ETOT12, respectively, and the out-of-plane rotation components of the panel skin, w,x and w,y, are assumed to be given by $k*w,x(0)$ and $k*w,y(0)$, where $w,x(0)$ and $w,y(0)$ are the rotation components corresponding to the initial local imperfection. These assumptions and substitutions into eqn (10) lead to three alternative values for k, as follows:

$$\text{from eqn (10a): } k(1) = -1 + \text{SQRT}[1 + 2*\text{ABS(ETOT1)}/w,x(0)**2]$$

$$\text{from eqn (10b): } k(2) = -1 + \text{SQRT}[1 + 2*\text{ABS(ETOT2)}/w,y(0)**2]$$

$$\text{from eqn (10c): } k(3) = -1 + \text{SQRT}[1 + \text{ABS(ETOT12)}/(w,x(0)*w,y(0))]. \quad (11)$$

The largest of the three $k(i)$ is chosen. It is called k(crit). The alternative local imperfection amplification factor WYYMP2 for nonhyperbolic amplification is given by

$$\text{WYYMP2} = 1 + k(\text{crit}). \quad (12)$$

The final amplification factor, WYYAMP, is chosen as the minimum of that given by Eq. (12) and the original "hyperbolic" value given by

$$\text{WYYAMP} = 1 + 1/(\text{lambda} - 1) \quad (13)$$

in which lambda is the load factor for local bifurcation buckling of the skin of the generally and locally imperfect panel.

INTRODUCTION OF PREBUCKLING AXISYMMETRIC BENDING INTO PANDA2

The "hungry horse" prebuckling deformation of ring stiffened cylindrical panels

Figure 1 shows axisymmetric prebuckling deformations obtained from a rather elaborate STAGS finite element model of a hydrostatically compressed, perfect, T-ring stiffened cylindrical shell. Three models of the shell/ring construction are used over the length of the shell, one in which the rings are "smeared", one in which the rings are modeled as discrete beams, and one in which the ring webs and flanges are modeled as flexible plates and shells. Notice in the two portions of the model where the rings are not "smeared" out that there is an axisymmetric waviness in the deformation pattern. This pattern is sometimes called "hungry horse" deformation because the locations of the ribs are apparent. In optimum designs the local axial bending stresses in the panel skin at the junctions with the webs of the ribs and midway between the ribs may become significant. Also, the hoop compression midway between the ribs may be significantly greater than that at the ribs, which affects local buckling load factors of the skin and of the rib web and outstanding flange. Until 1992 the "hungry horse" deformation was ignored in PANDA2.

Many changes were made to PANDA2 in order to obtain better results for the prebuckling states of cylindrical panels either unstiffened or with any combination of stringers and rings in which one of the loading components is normal pressure. Previously, PANDA2 produced a variety of results (some of them incorrect) depending on the circumferential angle spanned by the panel and the boundary conditions at the axially loaded ends of the panel.

Two important design problems motivated the changes in PANDA2: design of pressurized aircraft fuselages and design of submarine pressure hulls. With aircraft fuselages the pressure is internal, so that rather than a "hungry horse" prebuckling deformation there is a "caterpillar" deformation — the shell wall bulges outward more between rings than at rings.

There are three significant aspects of the modifications to PANDA2:

(1) The prebuckling static response of a cylindrical panel is now predicted from a theory similar to that given by Almroth [43] and by Jones and Hennemann [44]. This theory is outlined on p. 547, eqns (4)–(19) of Ref. [34]. It is included in the PANDA program, but until 1992 had not been included in the PANDA2 code. The theory is implemented differently in PANDA2 than in PANDA because conditions are needed at the ring stations (Subcase 2) as well as midway between rings (Subcase 1). In PANDA the conditions were determined only at the midbay locations, not at the ring stations. Therefore, the implementation in PANDA2 represents an improvement.

(2) When the panel is curved and there are rings present and there is pressure loading present, the two subcases per load set now correspond to conditions at midbay (halfway between adjacent rings, Subcase 1) and conditions at a typical ring location (Subcase 2). It is assumed that the two axially loaded ends (the two curved edges of the cylindrical panel) are free to approach or move away from each other. If the panel is stiffened by rings, prebuckling conditions at the ends of the panel are ignored. Previously the two subcases corresponded to conditions at the midlength and ends of the cylindrical panel and the user could choose whether or not the axially loaded (curved) edges are allowed to approach each other. In the modified code the user can still make this choice, but PANDA2 ignores the choice and allows the two curved edges to approach, or move away from each other as the pressure is applied. Textual output has been modified in PANDA2 to reflect these changes.

(3) In the MAINSETUP input the user is now forced to provide consistent values of the hoop loading (Ny or $Ny0$) and the pressure loading

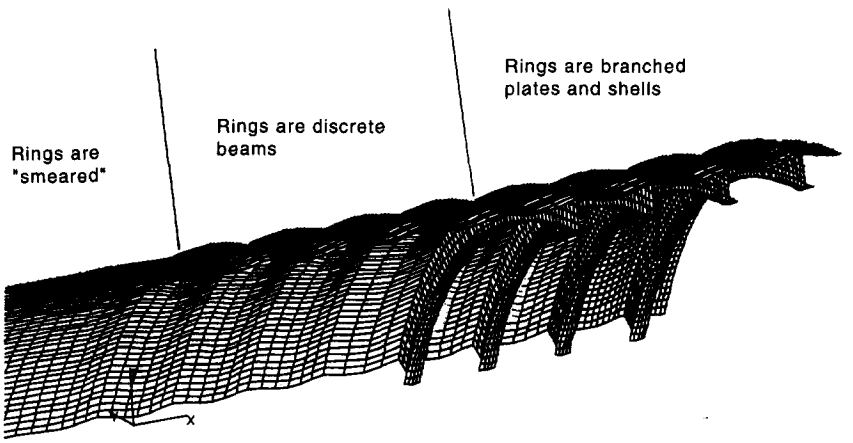

Fig. 1. STAGS finite element model of a perfect externally pressurized ring stiffened cylindrical shell.

whenever the panel is curved. Previously, under certain circumstances, the user was urged to represent the normal pressure loading with appropriate values for Nx or $Nx0$ and Ny or Nyo only, setting the pressure p equal to zero. This is no longer the case. If there is a nonzero hoop load in a curved panel, the user MUST now provide a consistent value for the normal pressure (so that free-body equilibrium is satisfied!). If consistent values of pressure and hoop loading (Ny or Nyo) are not provided the run aborts with the following warning:

********** RUN ABORT: BAD LOADS **********
THE PANEL IS CURVED. BAD LOAD DATA FOR LOAD SET NO. 1:
SEE FIG. 8 ON P. 490 OF THE LONG 1987 PAPER ON PANDA2 [34].
(1) If any hoop resultant (Ny or $Ny0$) is nonzero the
pressure p must be nonzero and must satisfy condition (2)
or (3) as follows;
(2) If the pressure is in Load Set A, then $p*R$ must be
equal to the hoop resultant in Load Set A, Ny.
(3) If the pressure is in Load Set B, then $p*R$ must be
equal to the hoop resultant in Load Set B, Nyo.
Radius of cylinder (positive as shown in Fig. 8), $R = 1.0000 \times 10^2$
NORMAL PRESSURE (positive acting upward), $p = -2.0000 \times 10^1$
Hoop load that must be applied for equilibrium, $p*R = -2.0000 \times 10^3$
Pressure is in Load Set A
CURRENTLY APPLIED HOOP LOADS, Ny(load set A) $= -1.5000 \times 10^3$
Nyo(load set B) $= 0.0000 \times 10^0$

The Almroth [43] and Jones and Hennemann [44] theory is implemented in SUBROUTINE SKIN, a new subroutine which is now contained in the STRUCT. NEW library and which is called from SUBROUTINE STRUCT if PANDA2 perceives that the panel is curved and normal pressure is present. There are differences in the way the theory is implemented in PANDA2 and the way in which it was originally implemented in PANDA.

The normal displacement distribution is not the same as that given in eqn (10) of Ref. [34]. The normal displacement distribution now has the form

$$w = wp0*[F1*\sin(a1*x)*\sinh(a2*x) + F2*\cos(a1*x)*\cosh(a2*x) + F3] \quad (14)$$

in which $F1$, $F2$, and $F3$ are undetermined coefficients, wpo is given by eqn (9) in Ref. [34], and $a1$ and $a2$ are given by eqn (11) in Ref. [34]. The domain of x is from the midbay (halfway between rings), where $x = 0$, to the ring station, where $x =$ (ring spacing)/2. Equation (14) satisfies the condition that the meridional slope $w,x = 0$ midway between rings (at $x = 0$). We know that at the ring station (at $x = A0/2$, where $A0 =$ ring spacing), $w,x = 0$ also. This condition yields $F2$ in terms of $F1$:

$$w,x = 0 \text{ at } x = A0/2 \quad \text{yields} \quad F2 = -\text{ARAT}*F1, \quad (15)$$

where ARAT is given in SUBROUTINE SKIN. Now the two unknowns are $F1$ and $F3$. These are determined from minimization of the total potential energy.

The total potential energy consists of the strain energy of the shell, the strain energy of the ring, the work done by the normal pressure, and the work done by the axial load, $Nx + Nx0$.

The strain energy of the shell is assumed to consist of membrane strain energy and bending strain energy. Because the static prebuckling response of the cylinder is assumed to be axisymmetric (there is no change in the curvature in the hoop direction and there is no in-plane shearing or twist), one can decouple the membrane and bending parts of the strain energy. The membrane part is independent of the location of the reference surface and the bending part is written with use of a reference surface located in the neutral plane for axial bending

$$C(4,4)(\text{neutral surface}) = C44N = C(4,4) - C(1,4)**2/C(1,1). \quad (16)$$

The membrane part of the strain energy is given by

$$U(\text{shell membrane}) = 2*pi*r*0.5*\text{integral}\{C11*e1**2 + 2C12*e1*e2 + C22*e2**2\}\,dx \quad 0 \text{ to } A0/2. \quad (17)$$

It is assumed in this analysis that the shell is free to expand or contract in the x-direction. Therefore,

the axial strain $e1$ can be expressed in terms of the axial resultant Nx and the hoop strain as follows:

$$e1 = (Nx - C12*e2)/C11. \tag{18}$$

Note that there is no $C14$ (bending–stretching coupling) term involved because we are using as a reference surface the natural plane for axial bending. For this reference surface the $C14$ term is zero. When eqn (18) is used to eliminate the axial strain $e1$ from eqn (17), and terms that do not depend on the unknowns $F1$ and $F3$ are dropped, the following simpler expression results for the membrane strain energy in the shell:

$$U(\text{shell membrane}) = 2*pi*r*0.5*\text{integral}\{C22 - C12**2/C11)*e2**2\}\,dx \quad 0 \text{ to } A0/2. \tag{19}$$

The hoop strain $e2$ is given by w/r, where w is given by eqn (14).

The bending strain energy in the shell is given by

$$U(\text{shell bending}) = 2*pi*r*0.5*\text{integral}\{C44N*(w,xx)**2\}\,dx \quad 0 \text{ to } A0/2. \tag{20}$$

The strain energy in the ring is given by

$$U(\text{ring}) = 2*pi*r*0.5*(EA/2)(w(x = A0/2)/r)**2 \tag{21}$$

in which EA is the ring hoop stiffness and r is the radius of the cylindrical shell. In eqn (21) $(EA/2)$ is used rather than EA because the ring lies at a plane symmetry. Therefore, only half of its hoop stiffness should be included in the strain energy.

The work done by normal pressure is given by

$$\text{Work(pressure)} = 2*pi*r*p*\text{integral}\{w\}\,dx \quad 0 \text{ to } A0/2. \tag{22}$$

The work done by the axial load Nx is given by

$$\text{Work (axial load)} = 2*pi*r*Nx*\text{integral}\{e1\}\,dx \quad 0 \text{ to } A0/2 \tag{23}$$

in which $e1$ is given by eqn (18). When the constant term is dropped, we obtain

$$\text{Work (axial load)} = 2*pi*r*Nx*(-C12/C11)*(1/r)*\text{integral}\{w\}\,dx \quad 0 \text{ to } A0/2. \tag{24}$$

When all these elements of the total potential are combined and the total potential $(U - W)$ is integrated and then minimized with respect to the unknowns $F1$ and $F3$, we obtain two linear simultaneous equations to be solved for $F1$ and $F3$. From eqns (14) and (15) we can then evaluate the normal displacements and the meridional changes in curvature (KAPPA1 = w, xx) midway between rings (at $x = 0$) and at the rings ($x = A0/2$). This is the information that is needed by the rest of PANDA2.

If during optimization the rings become very weak so that there is very little "hungry horse" bending in the prebuckling phase of the calculations, then PANDA2 performs the analysis only for the station midway between rings. Conditions at the rings are assumed to be so like those midway between rings that they are not calculated, and no margins are generated for Subcase 2. Essentially the number of subcases is reduced from 2 to 1.

If there are no rings, and if the user has indicated in the BEGIN processor that the panel is clamped along the curved edges for prebuckling calculations (IBPRE = 1), PANDA2 generates a very stiff ring at the panel end in SUBROUTINE SKIN only.

If there are no rings, and if the user has indicated in the BEGIN processor that the panel is "infinite" (infinitely along in the x-direction: IBPRE = 2), PANDA2 calculates the prebuckling solution ignoring the boundary conditions. That is, the panel deforms uniformly as if it were infinitely long. The prebuckling resultants are those calculated from statically determinate membrane theory. The number of subcases NCASES is set equal to one.

If the user has indicated in the BEGIN processor that the panel is simply supported at the axially loaded edges (the two curved edges in the cylindrical shell) and if there are no rings, the unknown $F2$ is determined in terms of $F1$ from the condition that $w, xx = 0$ at $x = A0/2$.

The "hungry horse" prebuckling deformation of the outstanding flange of the ring

In addition the "hungry horse" prebuckling axisymmetric deformations of the skin of the cylindrical shell, there is also a very local "hungry horse" axisymmetric deformation of the outstanding flange of each ring. Test runs with BOSOR4 on ring stiffened cylindrical shells optimized via PANDA2 demonstrate that this very local "hungry horse" deformation in the ring flange may be significant. Therefore, calculations have been introduced into SUBROUTINE SKIN in order to determine the meridional change in curvature WXXFLN in the ring flange at the intersection of ring web and outstanding ring flange. These calculations are performed if ICASE = 2 (PANDA2 is calculating conditions at the ring stations), ISTIF(2) = 1 (the rings have TEE-shaped cross-sections), and the length AXIAL of the cylinder is greater than 1.2 times the ring spacing $A0$. The following discussion provides an outline of the theory.

The outstanding ring flange is treated as a short cylindrical shell with an imposed radial displacement WRING at its midlength. This imposed radial displacement causes a local meridional change in curvature w,xx of the ring flange. The bending stresses from this can be significant, especially for composite materials.

The method is similar to that just completed for the panel skin: the axisymmetric normal displacement in the oustanding ring flange is written in the form

$$w = F1*\sin(a1*x)*\sinh(a2*x) + F2*\cos(a1*x)*\cosh(a2*x) + F3*\sin(a1*x)*\cosh(a2*x) + F4*\cos(a1*x)*\sinh(a2*x) + F5 \quad (25)$$

in which x is the coordinate measured along the generator of the short cylinder that is the ring flange. The quantity x is the coordinate direction normal to the ring web, with $x = 0$ at the intersection of the ring web and the ring flange, and x = WIDTH/2 at the curved edge of the ring flange (WIDTH = width of the outstanding ring flange).

At $x = 0$, w = WRING and the slope w,x is zero. At x = WIDTH/2, the curvature change w,xx is zero and the transverse shear Qx (w,xxx in this case) is zero. These four edge conditions are used to express $F2$, $F3$, $F4$ and $F5$ in terms of $F1$. Then $F1$ is determined by minimization of the strain energy in the flange which has an imposed normal displacement w = WRING at $x = 0$. The strain energy in the ring flange, which is treated now as a very short cylindrical shell of radius $r = R +$ HRING if the rings are external and $r = R$ — HRING if the rings are internal (HRING = height of the ring web), can be written in the form

$$U = 2*pi*r*0.5*\text{integral}\{(C22\text{star}/r**2)*w**2 + C44*w,xx**2\}\,dx \quad 0 \text{ to WIDTH}. \quad (26)$$

There is no work done by external forces. The undetermined coefficient $F1$ is calculated from the equilibrium condition $dU/dF1 = 0$, which leads to a single nonhomogeneous linear algebraic equation after the integration over x has been performed.

The analysis proceeds in a manner analogous to that for the panel skin. We are simply analyzing a different cylindrical shell with different boundary conditions and material properties.

In SUBCASE 1 PANDA2 uses the conditions at the midbay (halfway between two rings) to calculate buckling and stress, and in SUBCASE 2 PANDA2 uses the conditions at the rings. The meridional bending stress at these two stations is accounted for during optimization. If there are no rings, SUBCASE 1 corresponds to conditions at the midlength of the panel and SUBCASE 2 corresponds to conditions at the end of the panel.

The new prebuckling theory incorporated into PANDA2 has been verified via several runs with BOSOR4. A detailed example appears in the file PANDA2. NEWS [35].

If the panel is flat SUBROUTINE SKIN is not called.

ON SOME "TRICKS" CONCERNING IMPLEMENTATION INTO PANDA2

(1) During loading the amplitudes of the initial local, inter-ring, and general buckling modal imperfections grow in a manner that depends on both the buckling load of the perfect panel and the local, inter-ring and general collapse loads of the imperfect panel. An iterative method has been introduced into PANDA2 with quadratic extrapolation in order to predict the amplification factors, called WYYAMP(i), $i = 1, 2, 3$, for local, inter-ring, general imperfections. In order to prevent large oscillations of buckling load factors and stress from design iteration to iteration, any values of WYYAMP(i) larger than 4.0 are set equal to 4.0. Gradients of WYYAMP(i) with respect to perturbations in the decision variables are determined by

$$\text{WYYAMP(perturbed, } i) = \text{WYYAMP(unperturbed, } i)*\text{EIG(unperturbed, } i)/\text{EIG(perturbed, } i) \quad (27)$$

in which EIG represents the buckling load factor for the perfect panel.

(2) The load-carrying capacity of the imperfect panel is strongly dependent on the maximum radii of curvature of the imperfect panel in its loaded state. For example, the general instability load factor for an imperfect, axially compressed, cylindrical panel is strongly dependent on the local maximum circumferential radius of curvature. This local maximum circumferential radius of curvatures is a function of the amplitude of the general instability modal imperfection (in the panel as loaded, that is the initial amplitude plus its growth during loading) and the number of circumferential waves in the buckling mode. Test cases have shown that the use of only integral numbers of circumferential waves $(2, 3, 4, \ldots)$ for the prediction of the local maximum hoop radius of curvature may lead to very jumpy predictions during design iterations. The predictions from design iteration to iteration are considerably smoothed through the use of non-integral numbers of circumferential waves in the derivation of the local maximum circumferential radius of curvature of the imperfect panel. The non-integral number of waves is determined by quadratic interpolation of the buckling load factors predicted for three adjacent integral numbers of circumferential waves that includes the critical (minimum) buckling load factor. The non-

integral wave numbers are also used in the determination of curvature changes and twist.

(3) In the case of buckling of hydrostatically compressed ring stiffened cylindrical shells, there are two kinds of general buckling modes for a given number of circumferential waves, one mode with a single halfwave over the length of the cylinder (called "Mode 1") and another with many halfwaves over the length of the cylinder (called "Mode 2"). It often happens that optimum designs correspond to a configuration in which the load factors for these two very different mode shapes almost coincide. Since local buckling load factors and stresses depend very strongly on the general instability mode shape, these quantities may oscillate wildly from design iteration to iteration as Mode 1 and Mode 2 alternate as the critical general buckling mode. In order to avoid this difficulty, a new constraint condition has been introduced into PANDA2 that allows the user to force the mode with many axial halfwaves to be associated with a buckling load factor that is at least 5% higher than that corresponding to the mode with one axial halfwave. In the interactive MAINSETUP session the user is now asked,

Want to suppress general buckling mode
with many axial waves?

A "*Y*" response causes introduction of the new constraint condition.

(4) In most comparisons with results from STAGS for imperfect, hydrostatically compressed T-ring stiffened cylindrical shells, it has been found that collapse of the imperfect shell according to STAGS is caused by "ring tripping". In the neighbourhood of the circumferential location where occurs the maximum hoop compression in the outstanding flange of the ring (due to precollapse overall circumferential bending of the shell as the general imperfection is amplified under increasing load), the ring fails by "sidesway". The load at which ring tripping occurs can be significantly increased by forcing the outstanding flange of the ring to be wider than is its natural inclination during optimization. Making this flange wider can usually be achieved without significant gain in weight of the shell because material is reallocated throughout the structure as optimization cycles proceed. In PANDA2 better designs are now achieved because the factor of safety for ring tripping has been increased from 1.2 to 1.6.

(5) In order to compute knockdown factors corresponding to local, inter-ring, and general buckling, load factors for perfect and imperfect panels must be computed from the PANDA-type (closed form [34]) theory. The critical numbers of circumferential halfwaves for buckling of the perfect and imperfect panels can be very different. The question arises, which circumferential halfwavenumbers should be used in the determination of bending and twisting, w,xx, w,yy, w,xy, those for the perfect panel or those for the imperfect panel? The quantities, w,xx, w,yy, w,xy affect both buckling and stress. (For example w,yy for the general buckling mode affects the effective radius of curvature to be used for the analysis of local buckling of the imperfect panel.) As a result of comparisons with results from STAGS, it was found best to use the maximum numbers of circumferential halfwaves,

$$n(\text{crit}) = \max[n(\text{perfect}), n(\text{imperfect})] \quad (28)$$

in which n(perfect) represents the number of circumferential halfwaves in the critical buckling mode for the perfect panel and n(imperfect) represents that for the imperfect panel for whatever type of buckling (local, inter-ring, general) is being considered.

EXAMPLE 1: OPTIMUM DESIGN OF IMPERFECT MONOCOQUE CYLINDRICAL SHELLS

Figures 2–7 pertain to this section.

Figure 2–5 contain PANDA2 predictions for an aluminum cylindrical shell of length 100 in and radius 50 in. In the PANDA2 model the shell is represented as a panel that spans 180°. All four edges are simply supported. Each of the four figures 2–5 shows the evolution of thickness with design iteration for imperfect panels with several different amplitudes of general buckling modal imperfection *Wo*. In each figure the largest amplitude of imperfection corresponds to the thickest optimum design—a result to be expected. Several optimum designs are represented in each figure, one for each amplitude *Wo* (indicated by blackened points in Fig. 2, for example). Inserted into each of the four figures is a plot that gives the knockdown factors derived by PANDA2 at the optimum designs (called lambda1) as a function of normalized buckling modal imperfection amplitude, Wo/t.

Figure 2 shows results for uniform axial compression ($Nx = -1000\ \text{lb in}^{-1}$). There is reasonably good agreement of PANDA2 results with those from Koiter's special theory [45].

Figure 3 shows results for uniform axial compression ($Nx = -1000\ \text{lb in}^{-1}$) in the presence of internal lateral pressure. The internal pressure is assumed to exert no load on the end closures of the cylindrical shell (p generates no Nx). Four sets of results appear in the inserted plot: 1. Koiter's special theory (no internal pressure), 2. PANDA2 for the case with no internal pressure, 3. PANDA2 for the case with internal pressure in Load Set B, and 4. PANDA2 for the case with internal pressure in Load Set A. By "Load Set B" is meant a load set for which the loading is NOT to be multiplied by the eigenvalue (bucking load factor). In contrast, if the pressure is in "Load Set A" it is multiplied by the eigenvalue, that is, the pressure p varies in proportion to the axial load Nx. Note that, according to PANDA2, the load-carrying capacity of axially compressed internally pressurized cylindrical shells is considerably less sensitive to initial imperfections than unpressurized

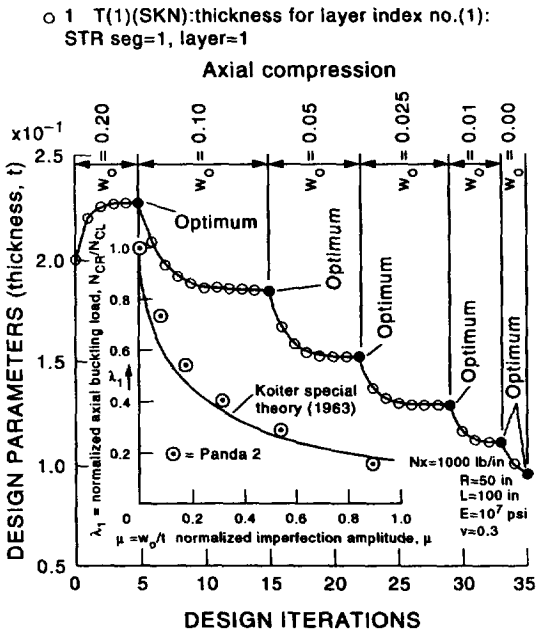

Fig. 2. Optimum designs of monocoque, aluminum, simply supported, axially compressed, imperfect cylindrical shells: $Nx = 1000\,\text{lb in}^{-1}$.

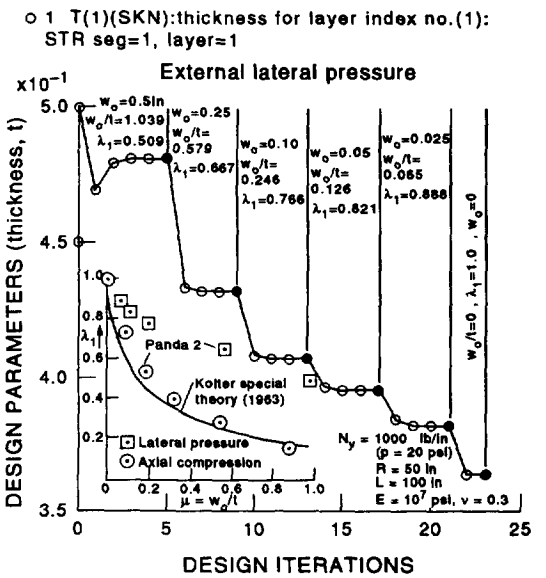

Fig. 4. Optimum designs of monocoque, aluminum, simply supported imperfect cylindrical shells subjected to external lateral pressure, $p = 20$ psi (no pressure on cylinder ends).

shells, if the amplitude of the buckling modal imperfection is less than about 2/3 of the thickness. The optimum designs of the imperfect pressurized shells are therefore thinner than those for the unpressurized shells. It should be emphasized that for the perfect shells the internal pressure has no influence on the optimum design provided that the stresses in the shell wall do not become critical during the optimization iterations.

Figures 4 and 5 give analogous results for the monocoque cylindrical shell loaded by uniform external lateral pressure (again, p generates no axial resultant Nx) and uniform torsion, respectively. For the torsion case some convergence difficulties with design iteration are encountered for the largest two imperfections, $Wo = 0.2$ in, and $Wo = 0.10$ in. The oscillation from design iteration to iteration, evident during iterations with $Wo = 0.2$ in, arises from wide swings in the imperfection amplification factor WYYAMP [eqn (13)] from iteration to iteration. The

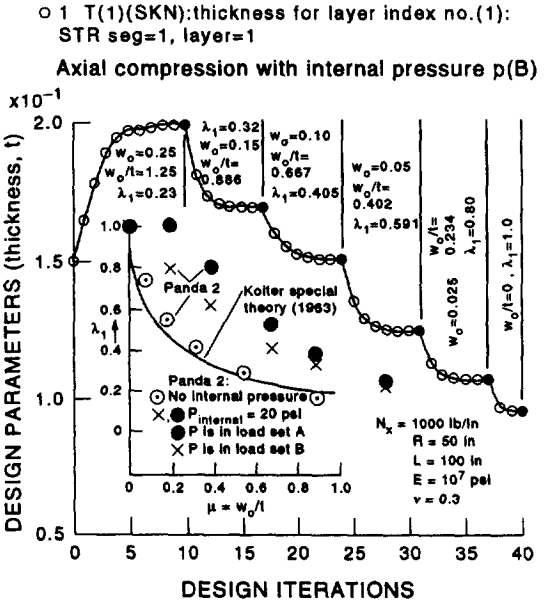

Fig. 3. Optimum designs of monocoque, aluminum, simply supported, axially compressed, imperfect cylindrical shells with internal pressure, $p = 20$ psi.

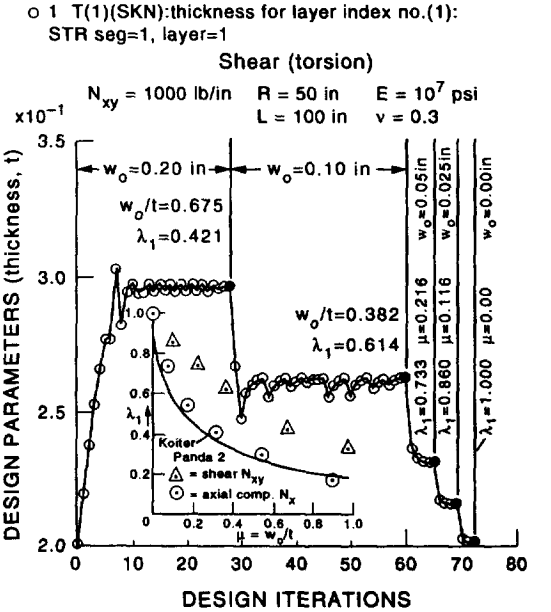

Fig. 5. Optimum designs of monocoque, aluminum, simply supported imperfect cylindrical shells subjected to torsion, $Nxy = 1000\,\text{lb in}^{-1}$.

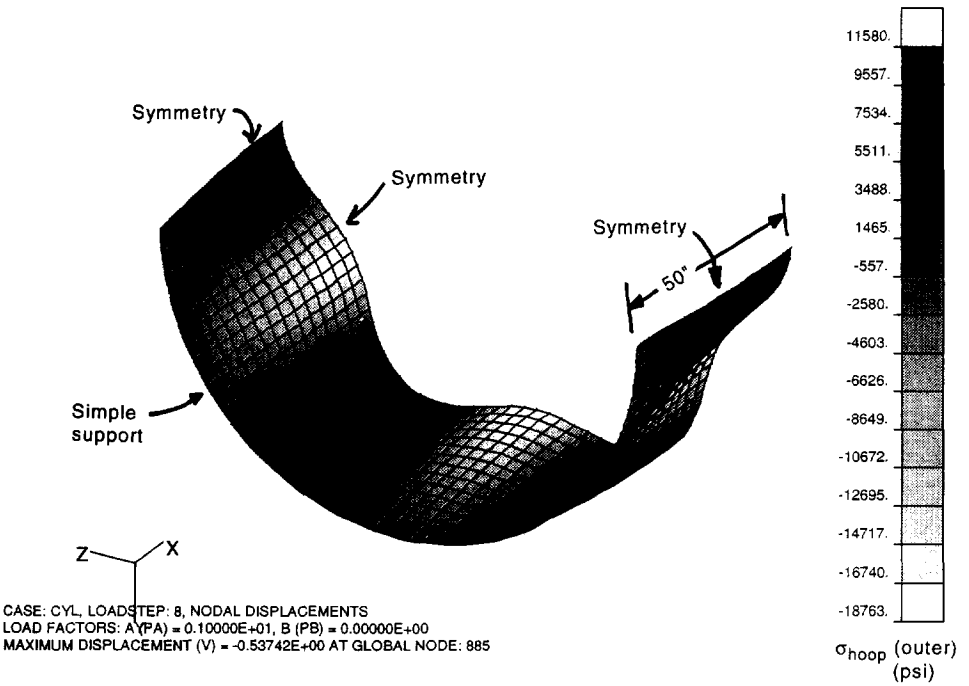

Fig. 6. Deformed state of optimized monocoque, aluminum, simply supported imperfect cylindrical shell subjected to external lateral pressure, $p = 20$ psi. Initial buckling modal imperfection amplitude, $Wo = 0.25$ in.

knockdown factors from PANDA2 for pure torsion indicate somewhat more imperfection sensitivity than does classical asymptotic theory, probably because of the assumption in the PANDA2 theory that the effective radius of curvature of the imperfect shell is everywhere equal to the minimum curvature.

Figures 6 and 7 show results from STAGS and a comparison between predictions by PANDA2 and STAGS for the optimized cylindrical shell (thickness, $t = 0.4318$) with uniform external lateral pressure and an initial buckling modal imperfection of amplitude $Wo = 0.25$ in. The STAGS results were generated from a model that includes 180° and half of the length of the cylindrical shell. The STAGS results shown in Figs 6 and 7 were obtained by first using STAGS to find the critical buckling mode from linear theory (INDIC = 1), including that mode as an initial imperfection with amplitude 0.25 in, and then running a STAGS nonlinear collapse analysis (INDIC = 3) of the imperfect shell. The agreement between PANDA2 and STAGS is reasonably good, with PANDA2 erring on the conservative side.

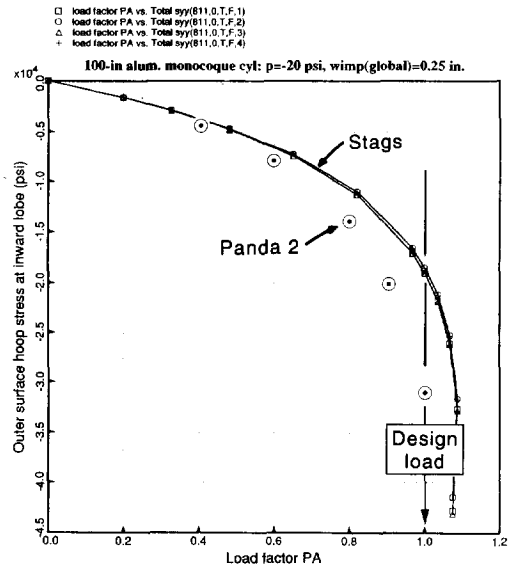

Fig. 7. Comparison of STAGS and PANDA2 predictions for optimized imperfect monocoque aluminum cylindrical shell.

EXAMPLE 2: OPTIMUM DESIGN OF AN IMPERFECT HYDROSTATICALLY COMPRESSED T-RING STIFFENED STEEL CYLINDRICAL SHELL

Figures 8–35 pertain to this section. The cylindrical shell is 70 in long and has a radius $R = 50$ in. It is made of steel with properties listed at the top of Fig. 8. The maximum allowable effective stress is 130 ksi. The internally ring stiffened shell is designed to withstand an ultimate external pressure of 150 psi. The design variables are the ring spacing b, web height h, outstanding flange width w, skin thickness $t(1)$, web thickness $t(2)$, and outstanding flange thickness $t(3)$. The initial imperfection in the form of the general buckling mode has an amplitude Wimp (global) = 0.25 in and the initial imperfection in the form of the local buckling mode has an amplitude Wimp (local) = 0.075 in. In PANDA2 the ring-stiffened cylindrical shell is modeled as a panel that spans 180°.

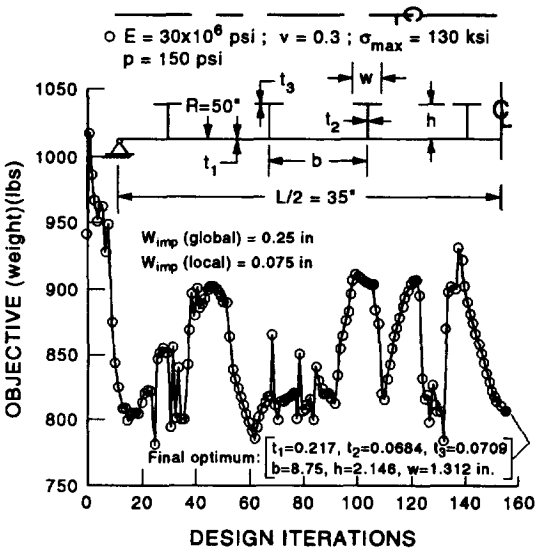

Fig. 8. Objective function (weight) of T-ring stiffened 70-in-long steel cylindrical shell under uniform external hydrostatic pressure, $p = 150$ psi.

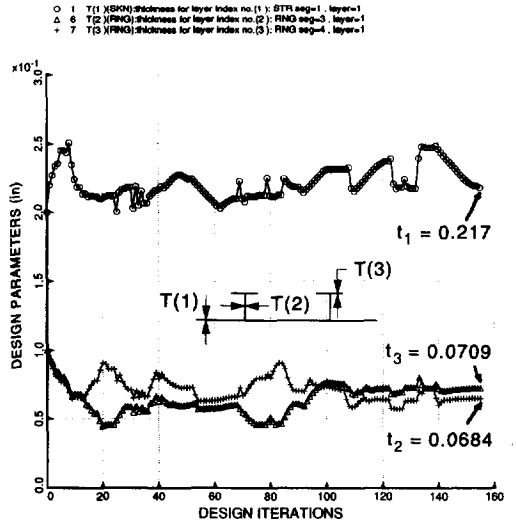

Fig. 10. Evolution of thicknesses of T-ring stiffened 70-in-long steel cylindrical shell under uniform external hydrostatic pressure, $p = 150$ psi.

PANDA2 model and optimization

Figures 8–12 show the evolution of the objective, of the design, and of the design margins with design iterations. For the first 20 iterations the ring spacing b was included as one of the decision variables. Thereafter, as seen in Fig. 9, b was held constant at various levels while all the other design variables were permitted to vary. It is often a good idea to perform several sets of optimization iterations with b held constant during each set because optimum weights for a rather wide range of b are usually very, very close to one another. PANDA2 therefore has an easier time finding optimum designs with b held constant during the design iterations. It is easy for the designer to use the PANDA2 processor called CHANGE in order to change b and explore several optima, each for a different fixed value of b.

In this case, even with the ring spacing b held constant within each of several design iteration loops, PANDA2 has a difficult time settling on optimum designs for each value of b. Figure 8 shows the objective function (weight) of the 180° panel vs iteration number from the start of the case. Note that the minimum weight that PANDA2 seems to be seeking is at about 800 lbs. However, every time this weight is approached, further iterations increase it temporarily, sometimes to a value exceeding 900 lbs. Figure 11 shows what is happening to the most critical design margins (all margins less than unity)

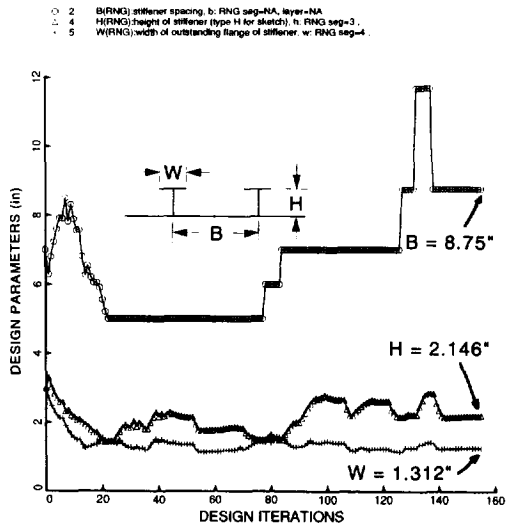

Fig. 9. Evolution of cross-section dimensions of T-ring stiffened 70-in-long steel cylindrical shell under uniform external hydrostatic pressure, $p = 150$ psi.

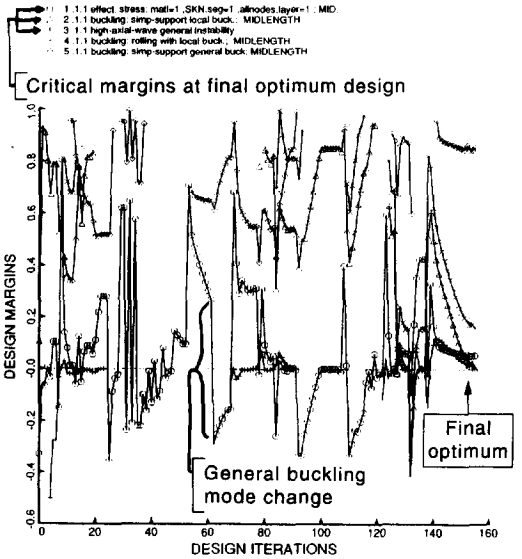

Fig. 11. Margins for the T-ring stiffened 70-in-long hydrostatically compressed steel cylindrical shell corresponding to conditions midway between adjacent rings.

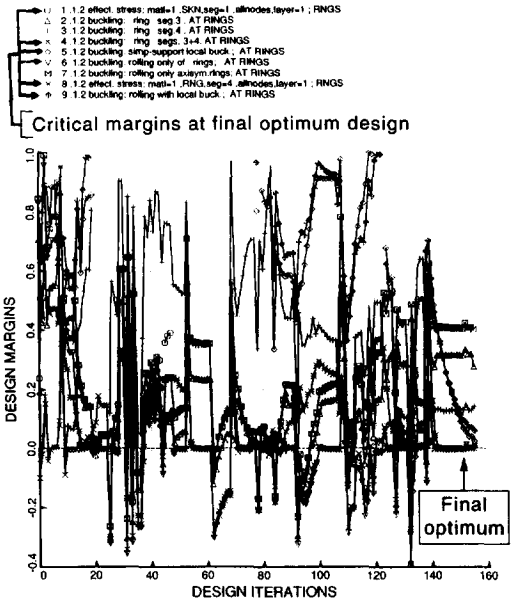

Fig. 12. Margins for the T-ring stiffened 70-in-long hydrostatically compressed steel cylindrical shell corresponding to conditions at a typical ring.

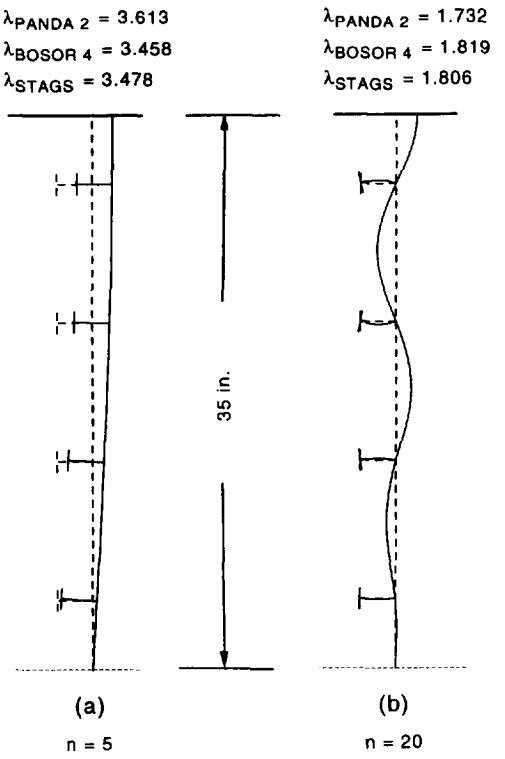

Fig. 13. Buckling mode shapes predicted by BOSOR4 and factors predicted by PANDA2, BOSOR4, and STAGS for the optimized, perfect 70-in-long hydrostatically compressed steel cylindrical shell: (a) general buckling mode; (b) local skin buckling mode.

corresponding to conditions midway between rings. For example, note the large jump in the effective stress margin from iteration number 61 to iteration number 62. (There are similar large jumps in this margin between iterations 25 and 35, at iteration number 83, at iteration number 91, and at iteration 108–110.) These large jumps are caused by a sudden change in the critical mode of general instability from Mode 1 to Mode 2, as described in paragraph no. 3 in the section entitled "On Some Tricks...". The mode with many axial halfwaves (Mode 2) leads to much higher bending stresses than that with only a

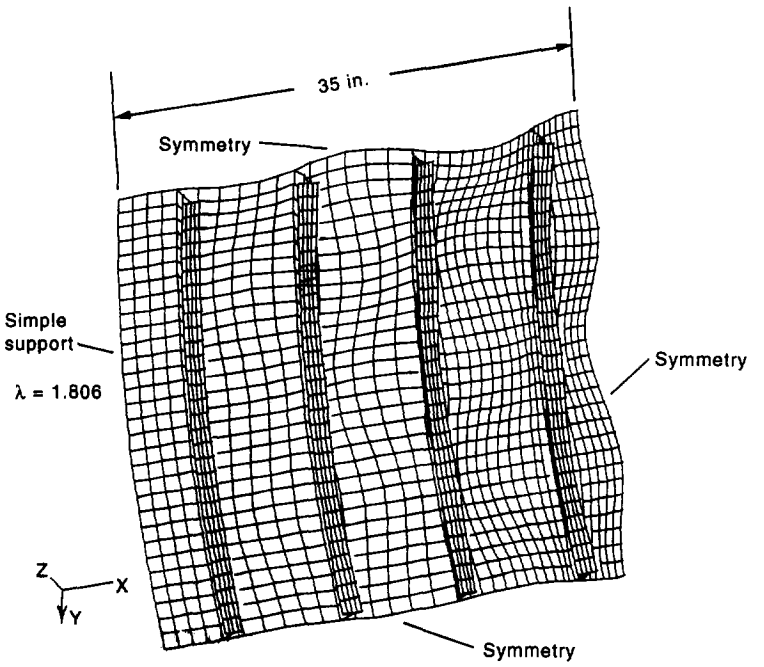

Fig. 14. Local skin buckling mode of the T-ring stiffened hydrostatically compressed 70-in-long steel cylindrical shell as predicted by STAGS.

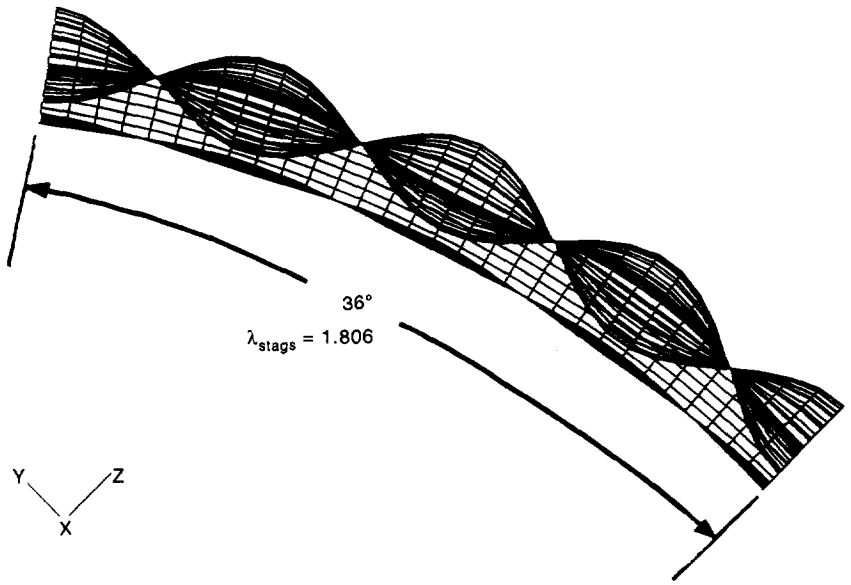

Fig. 15. Another view of the local buckling mode shown in the previous figure.

single axial halfwave (Mode 1). The margins for bucking of a web of a T-ring ("buckling of ring seg. 3") and for rolling of rings, displayed in Fig. 12, which corresponds to conditions at the rings, exhibit similar jumpy behavior because the prebuckling membrane stresses in the rings depend strongly on the general instability buckling mode shape, and these pre-local-buckling resultants govern local buckling and rolling of the rings.

The final optimum design chosen for analysis with BOSOR4 [46] and STAGS [39] is that corresponding to the highest iteration number. The dimensions of the optimum design appear at the bottom of Fig. 8.

BOSOR4 model of the panel optimized with PANDA2

Figure 13 shows the critical general and local buckling modes of the perfect shell predicted by BOSOR4 and the load factors predicted by PANDA2, BOSOR4 and STAGS. In the BOSOR4 model only half of the length of the shell is included, with symmetry conditions imposed at the symmetry plane of the shell. The critical general mode has five full waves around the entire (360°) circumference of the shell and the critical local mode has 20 full waves over 360°. Notice that the critical general mode is Mode 1, which has a single half wave over the full 70-in length of the cylindrical shell. There is good agreement of general and local buckling load factors predicted by all three computer programs.

STAGS model of the panel optimized with PANDA2

Figures 14–16 display the local and general buckling modes of the optimized perfect shell as predicted by STAGS. In the STAGS model half of the length and only 36° of circumference are included, with symmetry imposed along the three edges adjacent to the remainder of the shell and simple support imposed along the remaining curved edge. Only 36° of circumference are included because this sector permits general buckling with five circumferential halfwaves over 180° and also permits local buckling with 20 circumferential halfwaves over 180°. Computer times required for a 180° STAGS model would be excessive because a refined finite element mesh is required in order to capture the maximum local bending stresses in the panel skin with sufficient accuracy to qualify the STAGS model as a standard to be used to determine the suitability of the PANDA2 code as a tool for preliminary design.

Figures 14 and 15 show two views of the same local buckling mode and Fig. 16 shows the general buckling mode predicted by STAGS. These two modes are used as initial imperfections in a STAGS nonlinear collapse run. The amplitudes of the initial buckling modal imperfections are taken as Wimp (global) = 0.25 in and Wimp(local) = 0.075 in.

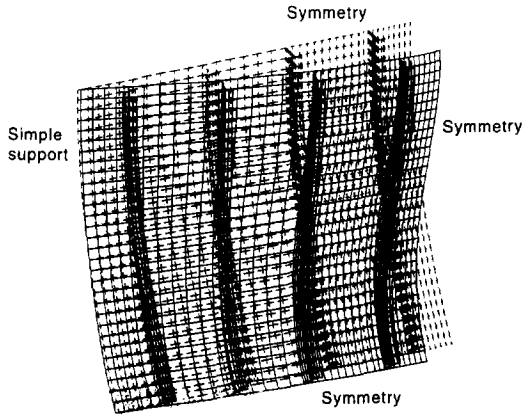

Fig. 16. General buckling mode of the T-ring stiffened hydrostatically compressed 70-in-long steel cylindrical shell as predicted by STAGS.

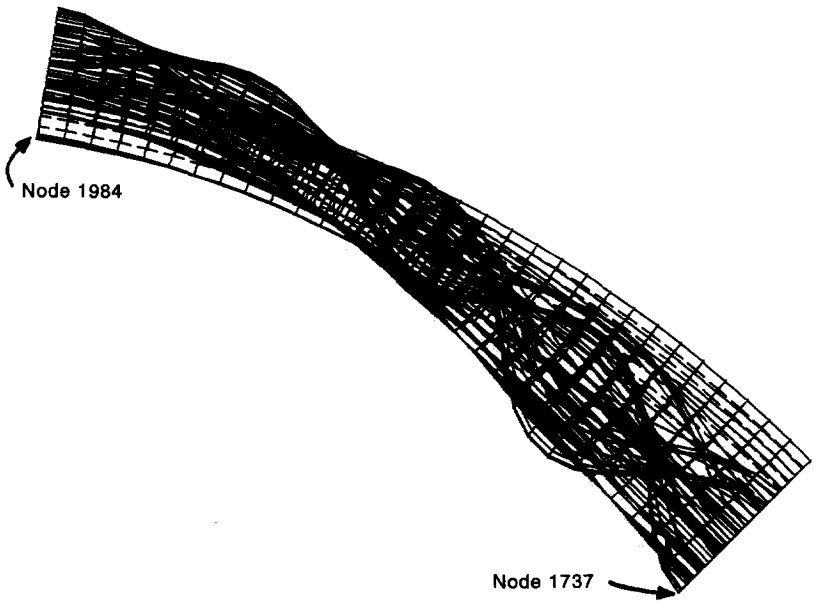

Fig. 17. Deformation of the imperfect steel shell at the design load, $PA = 1.0$, that is, at pressure $p = 150$ psi.

Figures 17–26 present results from the STAGS nonlinear collapse run, which required about 10 h on a STARDENT computer. Figure 17 is an end-on view of the deformed panel as loaded by the load factor $PA = 1.0$, which corresponds to the design load (external hydrostatic pressure $p = 150$ psi) in this and all further cases described in this paper. One can see that the overall deformation has two major components: overall bending with one half circumferential wave over the 36° sector (inward maximum displacement at one straight edge and outward maximum displacement at the other straight edge), and local bending with four half circumferential waves over the 36° sector. The amplitude of the local component of deformation is greatest where the skin is under the most circumferential compression

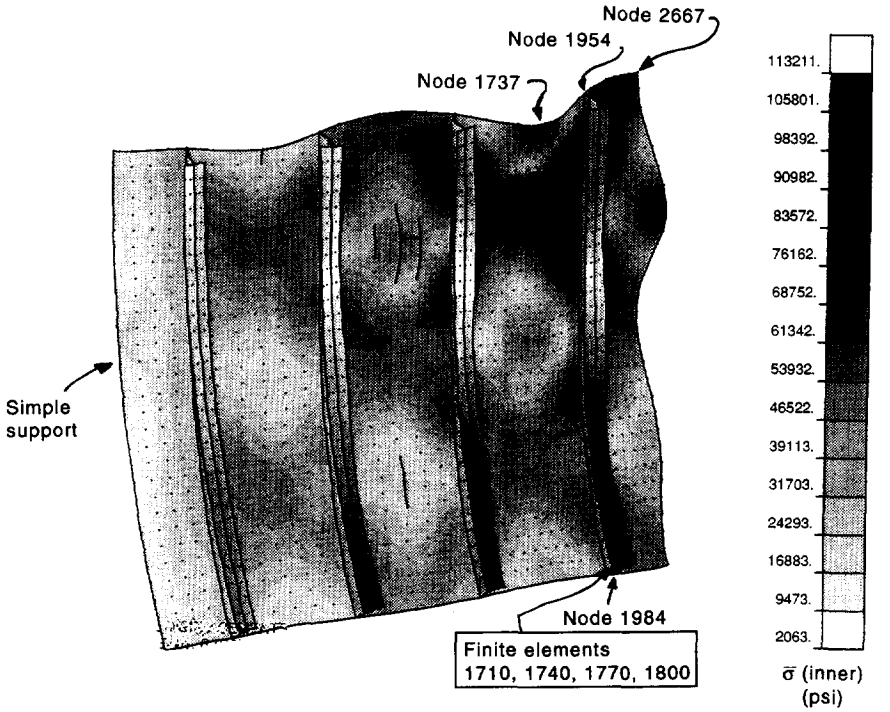

Fig. 18. Another view of the deformation of the imperfect steel shell, showing fringes of effective stress at the inner surfaces.

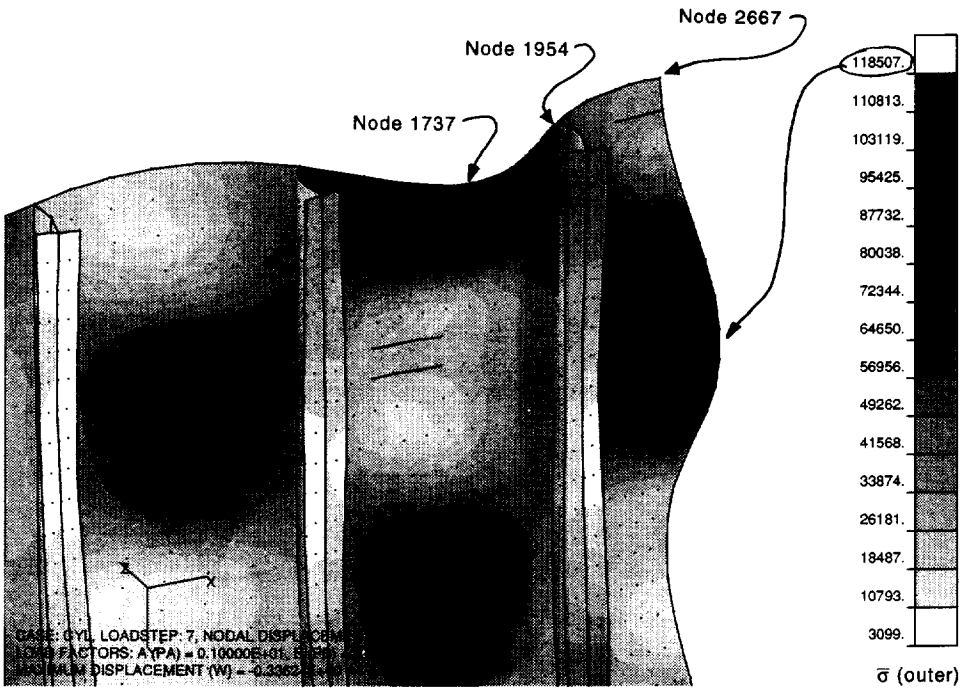

Fig. 19. Yet another view of the deformation of the imperfect steel shell, showing fringes of effective stress at the outer surfaces.

(right-hand side of the figure), as the entire shell bends circumferentially under the external pressure with both the general and local buckling modal components of the initial imperfection being therefore amplified. The overall inward displacement is greater than the overall outward displacement partly because there is a small overall average axisymmetric inward displacement component, since the cylindrical shell is subjected to uniform external pressure, and partly because the skin, being locally bent more where it is the most circumferentially compressed, has less effective hoop stiffness there than in the region

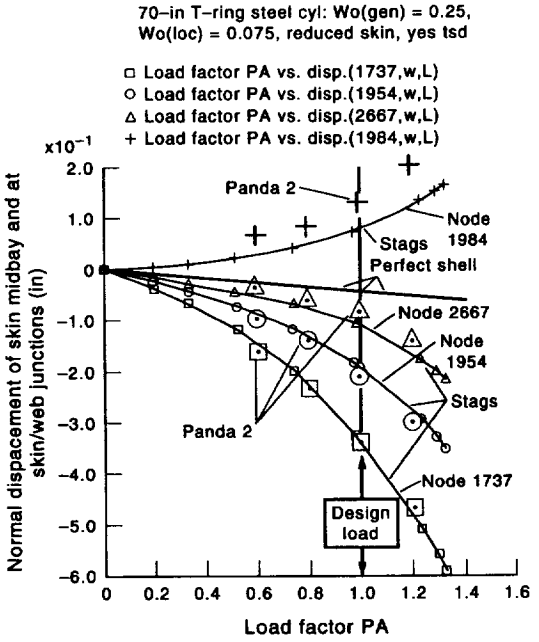

Fig. 20. Comparison of STAGS and PANDA2 predictions of normal displacement for the steel shell.

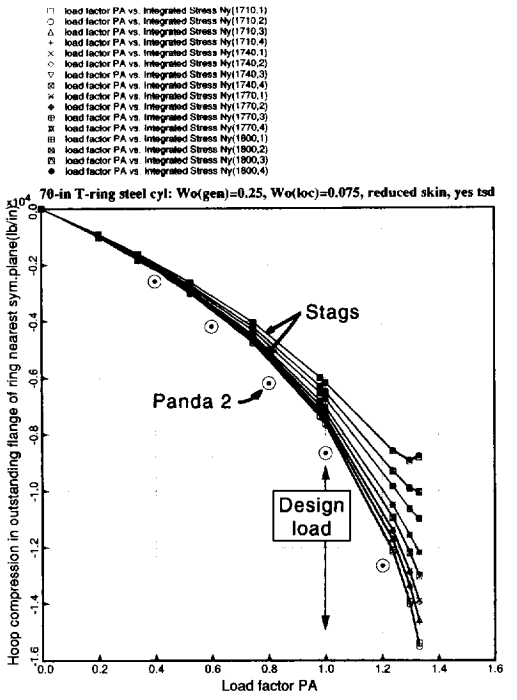

Fig. 21. Comparison of STAGS and PANDA2 predictions of hoop compression *Ny* in the ring flange of the steel shell where the flange is compressed more than the skin.

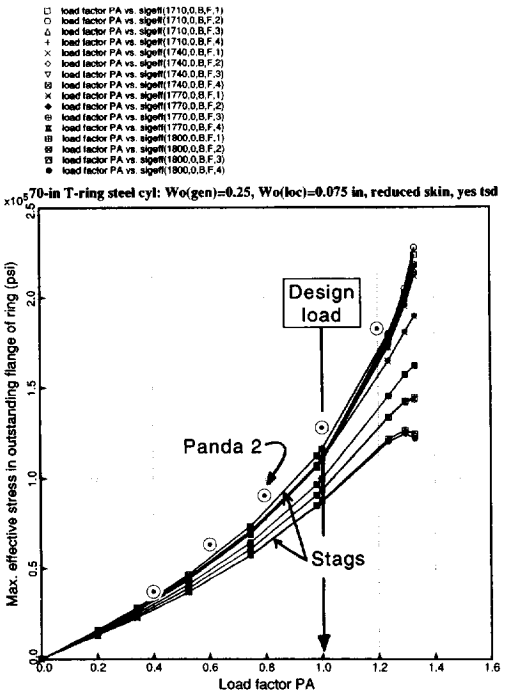

Fig. 22. Comparison of STAGS and PANDA2 predictions of effective stress in the ring flange of the steel shell where the flange is compressed more than the skin.

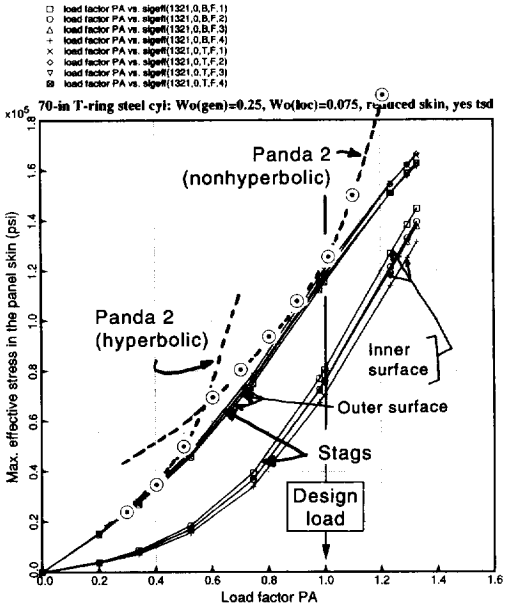

Fig. 23. Comparison of STAGS and PANDA2 predictions of effective stress in the panel skin of the steel shell where the skin is compressed more than the outstanding flange of the ring.

near the opposite straight edge where the skin is compressed less than the outstanding flanges of the rings.

Figures 18 and 19 are PATRAN [47] fringe plots of the inner and outer surface effective stress in the panel as loaded by the design load, $p = 150$ psi. These figures show the overall displacement pattern. The actual displacement field is magnified in the plots by a scale factor of 20. The upper right-hand portion of the model has the maximum overall inward displacement. It is obvious from Fig. 18 that the initial local buckling modal imperfection is most amplified in the region with the maximum overall inward bending. The maximum inner fiber effective

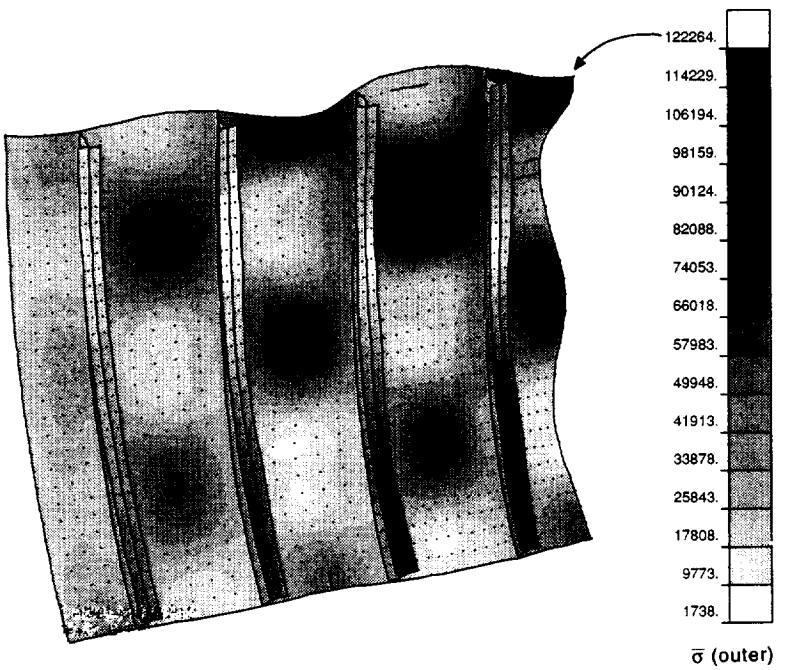

Fig. 24. Deformed shape and fringes of outer surface effective stress in the steel shell from a model in which the sign of the local buckling modal imperfection component has been changed.

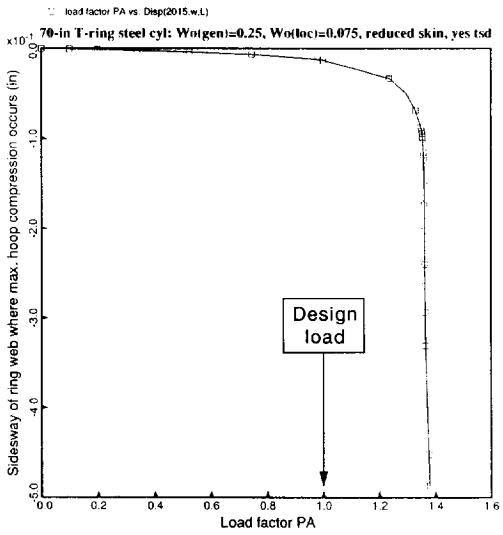

Fig. 25. Ring tripping in the imperfect steel shell.

stress occurs in the outstanding flange of the ring nearest node 1984. The maximum outer fiber effective stress occurs in the panel skin at both of the inward directed local "bumps" most clearly displayed in Fig. 19.

Comparisons of results from PANDA2 and STAGS

Figures 20–23 give comparisons between results from PANDA2 and STAGS. In Fig. 20 are plotted the normal displacement w at the four nodal points 1737, 1954, 1984, and 2667 (locations shown in Figs. 18 and 19). Nodes 1954 and 1984 are at the junction of web and skin of the ring nearest the midlength symmetry plane of the cylindrical shell at the points of maximum inward and outward displacement, respectively. Nodes 1737 and 2667 are at midbay in the panel skin at the points of maximum local inward and outward displacement, respectively. The straight line labelled "perfect shell" represents the average overall inward axisymmetric displacement caused by the uniform external hydrostatic compression.

In the PANDA2 model a reduced effective skin stiffness is used (indicated as "reduced skin" in the title over the plot), and the effects of transverse shear deformation are included (indicated as "yes tsd" in the plot title). In the "reduced skin" PANDA2 model the membrane components of the integrated constitutive 6×6 matrix (called $C(1,1)$, $C(2,2)$, and $C(3,3)$ in the PANDA2 literature and termed $A11$, $A22$, $A33$ in most of the literature on composite materials) for the panel skin are set equal to half of the values corresponding to the perfect skin. The PANDA2 user can choose whether or not to use the "reduced skin" and "yes tsd" options for deriving optimum designs. It is advisable to do so in order to derive conservative designs. The effective overall membrane stiffness of the skin is reduced because of the presence of the local imperfection. Later, results from PANDA2 with and without the "reduced skin" and "tsd" options are explored for ring stiffened cylindrical shells made of laminated composite material.

Figures 21–23 give comparisons between PANDA2 and STAGS predictions for the maximum hoop compression in the outstanding ring flange and maximum effective stress in the ring flange and panel skin. The agreement between results from PANDA2 and STAGS is very good. In each of Figs 21 and 22 there is only one curve corresponding to the PANDA2 model, whereas there are many corresponding to the STAGS model. Unlike the STAGS model, in the PANDA2 model there is no twisting of the ring as the local buckling modal

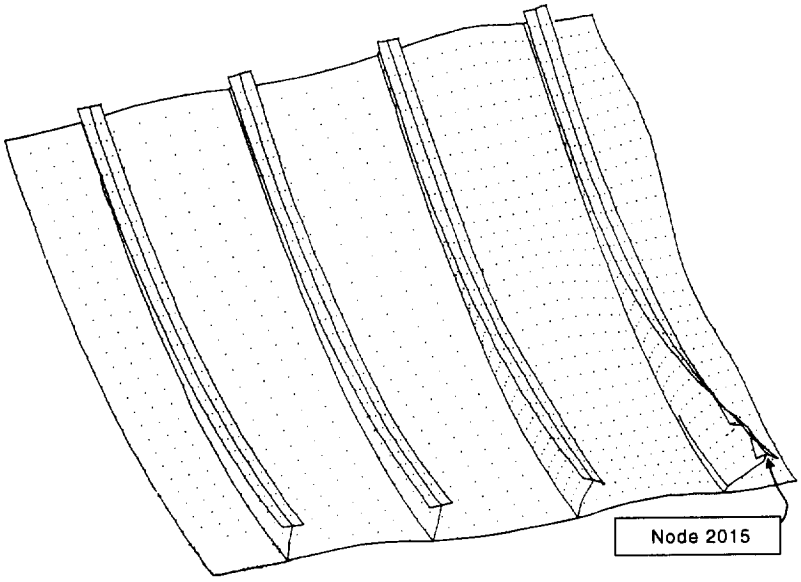

Fig. 26. Deformed shape in the post-collapse regime.

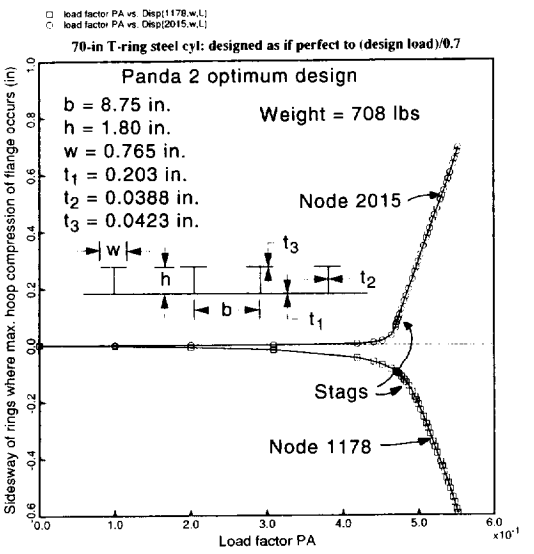

Fig. 27. Early ring tripping in steel shell optimized as if it were perfect to a design pressure, $p = 150/0.7 = 214.28$ psi. The width of the flange is too small.

imperfection is amplified. In the PANDA2 model it is as if the rings were hinged along their lines of intersection with the panel skin. Therefore, the rings do not twist as the local buckles deepen with increasing external pressure. It is the twisting of the rings that gives rise to the variation of hoop stress across the width of the outstanding flange. The ring twisting would be included if there were a discretized skin-ring single module model in PANDA2 analogous to the skin-stringer single module model shown in Fig. 98a of [32], for example.

In Fig. 23 it is indicated whether the amplification of the initial local buckling modal imperfection is governed by the hyperbolic law, eqn (13), or the nonhyperbolic law, eqn (12), in the PANDA2 analysis. The transition between hyperbolic and nonhyperbolic amplification depends on the amplitude of the initial local imperfection and its circumferential wavelength, as well as on the properties of the panel skin and whether or not the stress in the skin and/or the local buckling load factor for the imperfect shell are critical or nearly so. For small applied loading the amplification of the local buckling modal initial imperfection is always hyperbolic and above the local buckling load of the imperfect shell it is always nonhyperbolic.

Figure 24 shows the outer surface effective stress from a STAGS model in which the sign of the local initial imperfection has been reversed and all other properties of the STAGS model maintained as before. This figure should be compared with Fig. 19. Note that the maximum effective stress predicted from the second model is only slightly greater than that from the first.

Figures 25 and 26 demonstrate that collapse of the shell is caused, according to STAGS, by sidesway of the T-ring in the region where the outstanding ring flange is subjected to maximum hoop compression. This is called "ring tripping". It is the ultimate cause of failure of the structure in all of the cases explored here except two.

Various optimum designs obtained for the same T-ring stiffened cylindrical shell with no initial imperfections

In earlier literature on the optimum design of stiffened panels and shells [32, 34] it is recommended

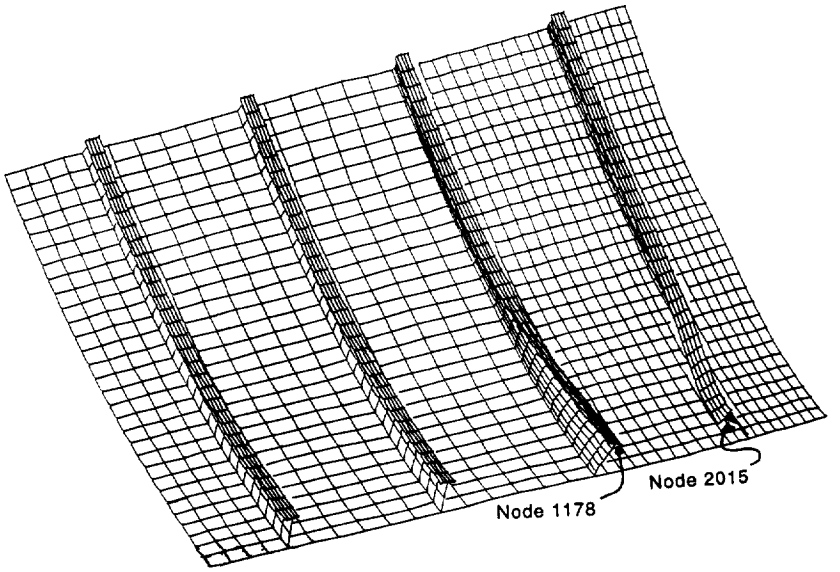

Fig. 28. Deformed shape in the post-collapse regime of the steel shell optimized as if it were perfect to a design pressure, $p = 150/0.7$ psi.

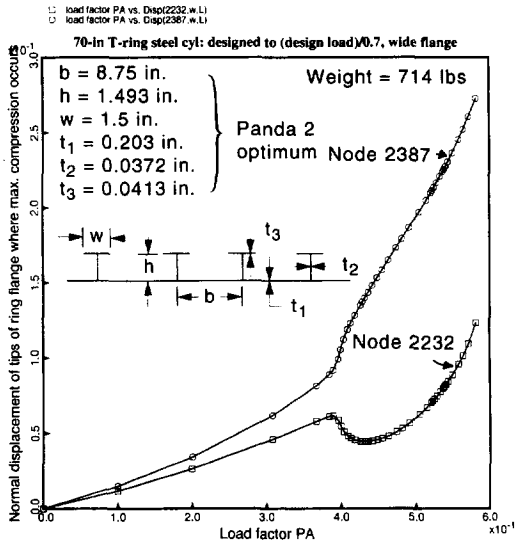

Fig. 29. Early ring cross-section buckling and crippling in steel shell optimized as if it were perfect to a design pressure, $p = 150/0.7$ psi. A lower bound on the width of the outstanding ring flange of 1.5 in was imposed during optimization, but the thicknesses of web and flange are too small.

to account for initial imperfections by designing the perfect shell to a higher load than the ultimate load. It is recommended, for example, that the perfect shell be designed to withstand the applied load given by

$$\text{(Design load of perfect shell)} = \text{(ultimate load)/(knockdown factor)} \quad (29)$$

in which the knockdown factor supposedly compensates for initial imperfections. The following results demonstrate that this philosophy is unsafe. Figures 27–35 pertain to this section. In each case the structure is assumed to be perfect and it is designed to withstand an external hydrostatic pressure equal to $(150)/(0.7) = 214.28$ psi. The knockdown factor of 0.7 is typical for use with cylindrical shells under external pressure.

Figures 27 and 28 give results from STAGS for the optimum design obtained with PANDA2 for the perfect shell designed to withstand the higher external pressure, $p = 214.28$ psi. The STAGS results correspond to an imperfect shell with the same general and local imperfection amplitudes as before, Wimp (global) = 0.25 in and Wimp(local) = 0.075 in. As before, the load factor $PA = 1.0$ corresponds in the STAGS model to an external pressure $p = 150$ psi, not the higher pressure, $p = 214.28$ psi, used in the PANDA2 analysis to obtain the optimum design of the perfect shell.

Figure 27 lists the dimensions and weight of the optimum design obtained by PANDA2 and demonstrates sidesway ("ring tripping") of the T-ring that begins at a load of less than half of the design load of 150 psi. The mode of collapse of the structure is depicted in Fig. 28. (In this case the STAGS model spans 30° of the circumference because PANDA2 predicts general buckling with six circumferential halfwaves over 180° rather than the five halfwaves that is critical for the optimum design discussed in the previous section.) The optimum design produced for the perfect shell designed to the higher pressure, $p = (\text{design load})/0.7$, is inadequate because the flange is too narrow to resist the ring tripping that is predicted by STAGS to

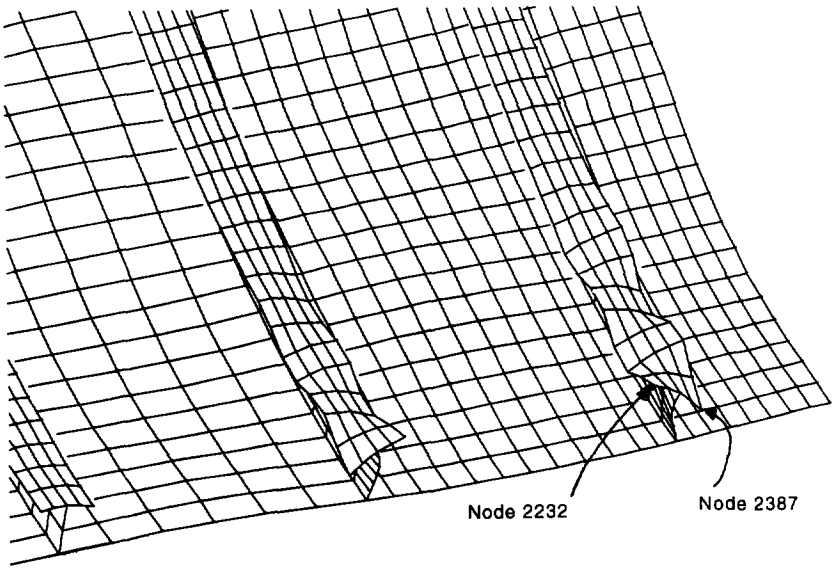

Fig. 30. Deformed shape in the post-collapse regime of the steel shell optimized as if it were perfect to a design pressure, $p = 150/0.7$ psi.

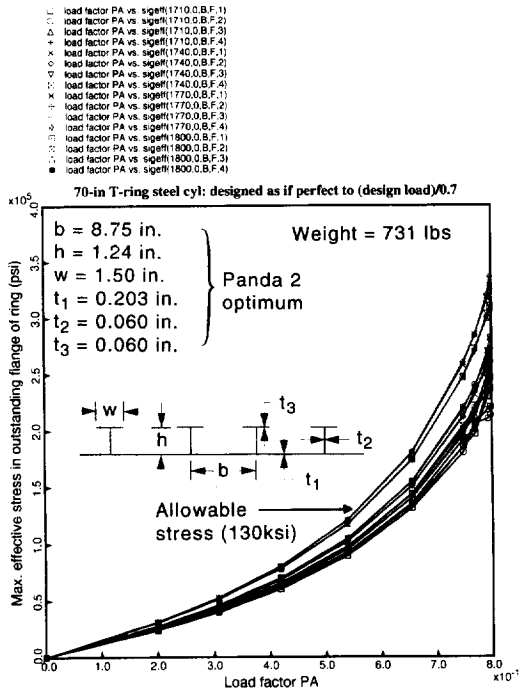

Fig. 31. Early stress failure caused by excessive overall bending in steel optimized as if it were perfect to a design pressure, $p = 150/0.7$ psi. Lower bounds on the width of the outstanding ring flange and thicknesses of web and flange were imposed during optimization, but the height of the web is too small.

occur when imperfections of reasonable amplitude are included explicitly in the STAGS model. (PANDA2 predictions for this optimum design agree with those of STAGS when the same initial imperfections are included explicitly in the PANDA2 model).

A new warning is generated in the PANDA2 output file, *.OPM, if a cylindrical shell or panel with rings is being optimized without any out-of-roundness or general buckling modal initial imperfection. The warning is as follows:

In view of the results shown in Figs 27 and 28, it is reasonable to perform the PANDA2 optimization for the perfect shell again, this time enforcing a lower bound on the width of the outstanding flange of 1.5 in in order to forestall ring tripping. The results from PANDA2 and STAGS appear in Figs 29 and 30. This time failure of the structure is caused by local buckling and crippling of the cross-sections of the T-rings rather than by ring tripping. Local buckling of the T-rings initiates at a load factor of about 0.4, again, less than half the design pressure, $p = 150$ psi.

In view of the results shown in Figs 27–30, it is reasonable to perform the PANDA2 optimization for the perfect shell yet again, this time enforcing a lower bound on the width of the outstanding flange of 1.5 in and lower bounds on the thicknesses of the ring web and flange of 0.06 in. The results appear in Figs 31 and 32. This time failure occurs because of overall collapse, as shown in Fig. 32. The effective stress in the outstanding flange of the T-ring exceeds the allowable value of 130 ksi at only 60% of the design pressure $p = 150$ psi.

In view of the results shown in Figs 27–32, it is reasonable to perform the PANDA2 optimization for the perfect shell yet again, this time enforcing a lower bound on the height of the T-ring of 2.0 in and the same lower bounds on width of outstanding flange and thicknesses of ring web and flange as listed in the previous paragraph. The results appear in Figs 33–35. Figure 33 lists the optimum design and weight determined by PANDA2. Results from a STAGS model of the panel optimized with PANDA2 are shown in Figs 33–35. This panel collapses at a load above the design load, but the maximum effective stress at the design load, $PA = 1.0$, that is, at the design pressure of 150 psi, exceeds the allowable by about 30%. Figures 34 and 35 are PATRAN fringe plots of the effective stress at the locations where the outstanding flanges of the rings are compressed the most (Fig. 34) and where the panel skin undergoes the most bending (Fig. 35). The shell is only about 7% lighter than the acceptable design, results for which

******** WARNING ******** WARNING ******** WARNING ********
THE PANEL IS CURVED, HAS RINGS, YET HAS NO OVERALL IMPERFECTION.
OVERALL IMPERFECTIONS (OUT-OF-ROUNDNESS AND/OR BUCKLING
MODAL IMPERFECTION) GIVE RISE TO CONSIDERABLE ADDITIONAL HOOP
COMPRESSION IN THE RING WEBS AND OUTSTANDING FLANGES, AS WELL
AS IN THE PANEL SKIN. PLEASE NOTE THAT, EVEN THOUGH YOU MAY
HAVE SET THE APPLIED LOAD TO A VALUE HIGHER THAN THE DESIGN
ULTIMATE LOAD BY A FACTOR EQUAL TO THE INVERSE OF A TYPICAL
KNOCKDOWN FACTOR, OR YOU MAY HAVE SET A RATHER HIGH FACTOR OF
SAFETY FOR GENERAL INSTABILITY, YOUR DESIGN MAY BE UNCONSERVATIVE.
PLEASE REDESIGN WITH USE OF REASONABLE AMPLITUDE(S)
FOR OUT-OF-ROUNDNESS AND/OR GENERAL BUCKLING MODAL IMPERFECTION.
YOU MAY COMPENSATE BY REDUCING THE FACTOR OF SAFETY
AND/OR THE APPLIED LOAD (AS LONG AS THE APPLIED LOAD REMAINS
AT LEAST AS LARGE AS THE ULTIMATE LOAD).
****** END WARNING ***END WARNING ***** END WARNING ********

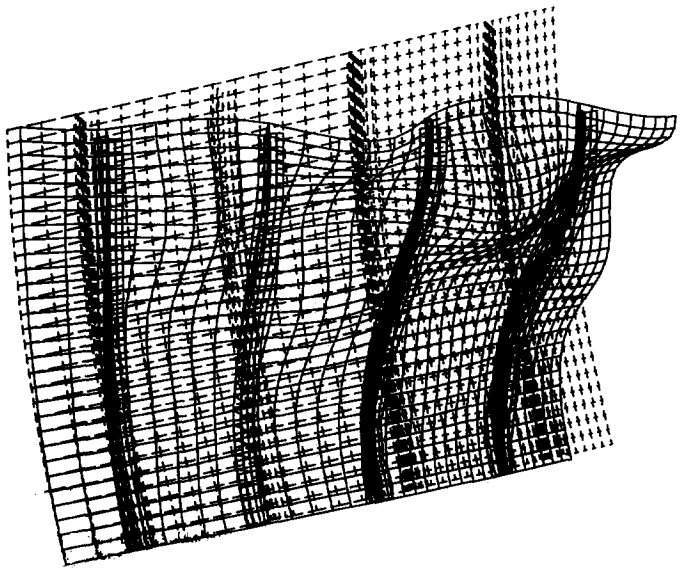

Fig. 32. Deformed shape in the post-collapse regime of the steel shell optimized as if it were perfect to a design pressure, $p = 150/0.7$ psi.

appear in Figs 14–26. It is easy to imagine that 7% might have to be added to the weight in order to bring the maximum effective stresses below the allowable value of 130 ksi at the design pressure, $p = 150$ psi.

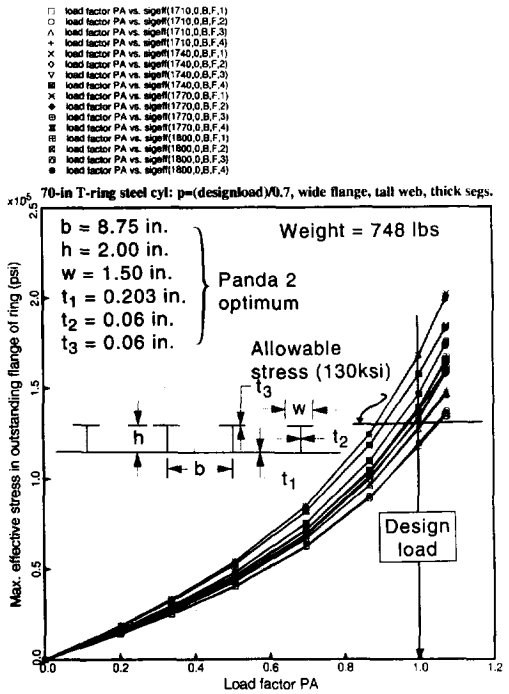

Fig. 33. Early stress failure caused by excessive overall bending in steel shell optimized as if it were perfect to a bending pressure, $p = 150/0.7$ psi. Lower bounds on the width of the outstanding ring flange, thicknesses of the web and flange, and a lower bound of 2.0 in on the height of the web were imposed during optimization, but the maximum allowable stress of 130 ksi is still exceeded at the design load.

EXAMPLE 3: OPTIMUM DESIGN OF AN IMPERFECT HYDROSTATICALLY COMPRESSED T-RING-STIFFENED COMPOSITE CYLINDRICAL SHELL 70 INCHES LONG

Figures 36–56 pertain to this section. As with the steel T-ring stiffened shell, the cylindrical shell is 70 in long and has a radius $R = 50$ in. It is made of laminated composite material with properties listed in Figs 36 and 37. As before, the ring stiffened shell is designed to withstand an ultimate external hydrostatic pessure of 150 psi. The design variables are the ring spacing b, web height h, outstanding flange width w, the lamina thicknesses $t(1)$, $t(2)$, $t(3)$, $t(5)$, $t(6)$, $t(8)$ and $t(13)$. The thickness $t(4)$ is linked to $t(3)$, since these are the plus and minus 45° layers in Laminate 1, which forms the panel skin. The thickness $t(7)$ is linked to $t(6)$, since these are the plus and minus 45° layers in Laminate 2. The thickness $t(14)$ is held at the value of a single ply, 0.005 in, because it represents each of the 90° layers in Laminate 3, which forms the core of the ring outstanding flange. As before, the initial imperfection in the form of the general buckling mode has an amplitude Wimp(global) = 0.25 in and the initial imperfection in the form of the local buckling mode has an amplitude Wimp(local) = 0.075 in. In PANDA2 the ring-stiffened cylindrical shell is again modeled as a panel that spans 180°. In contrast to the ring-stiffened steel shell discussed in the previous section, the composite ring-stiffened shell has rings with faying flanges. The width of the faying flange is kept constant at 1.5 in, as shown in Fig. 36.

PANDA2 model of the composite panel and optimization

Figures 37–41 are analogous to Figs 8–12. They show the evolution of the design and of the design

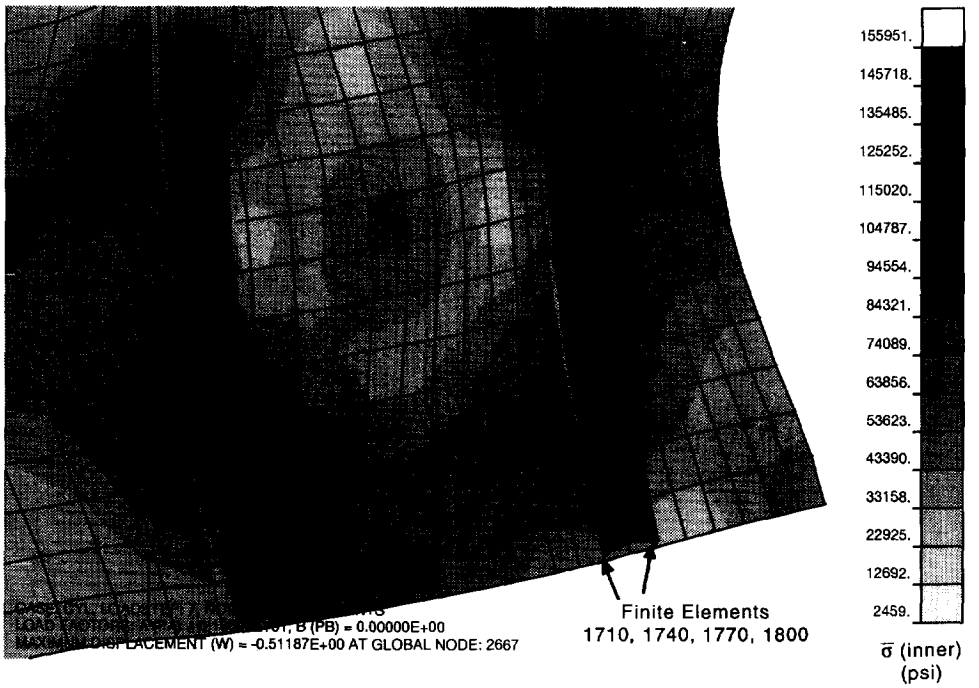

Fig. 34. PATRAN fringe plot of the inner surface effective stress in the region where the outstanding flanges of the rings are compressed the most.

margins with design iterations. For the first 55 iterations the ring spacing b was included as one of the decision variables. Thereafter, as seen in Fig. 38, b was held constant at various levels while all the other design variables were permitted to vary. The optimum design weighs only 38% as much as the optimized steel shell (compare Figs 8 and 37).

During most design iterations the thicknesses $t(1), t(2), t(3), t(5), t(6), t(8), t(13)$, are permitted to vary in an arbitrary way. However, in the final optimum design each layup angle must consist of an

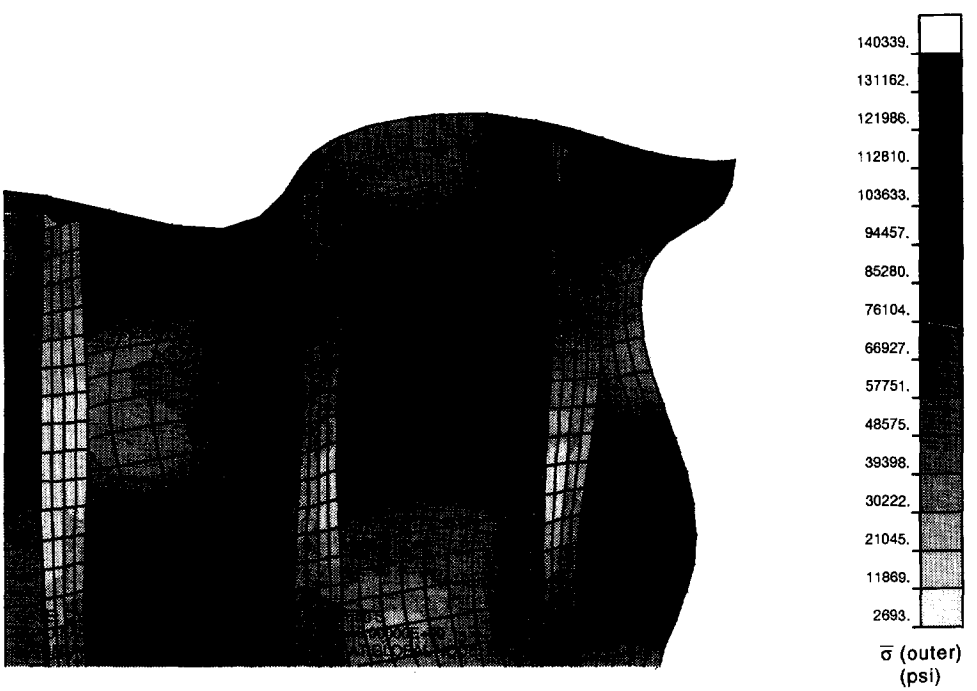

Fig. 35. PATRAN fringe plot of the outer surface effective stress in the region where the skin undergoes the most bending.

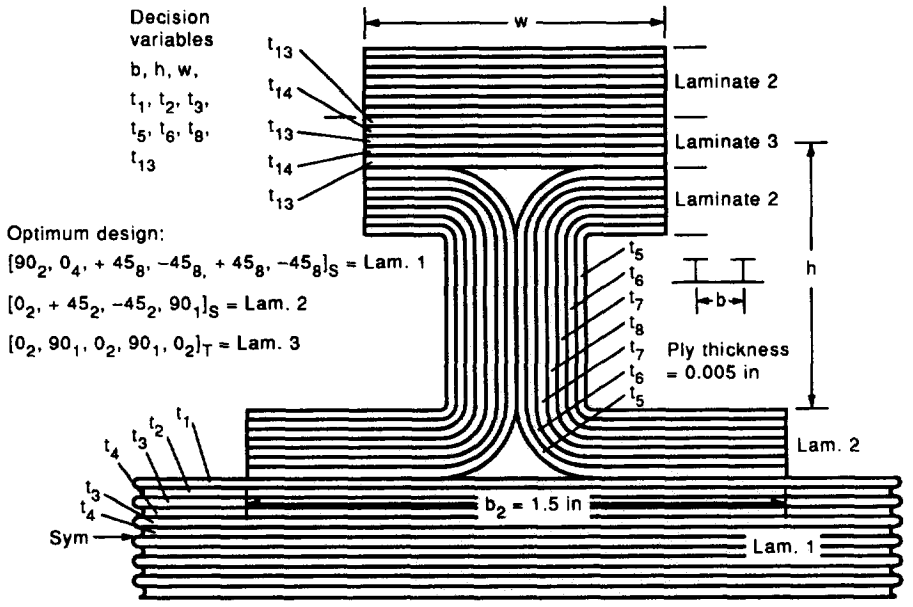

Fig. 36. Layup scheme for all of the laminated composite T-ring stiffened cylindrical shells treated in this paper. Optimum ply distribution for the 70-in-long cylindrical shell optimized with "reduced skin" and "tsd" switches turned on during optimization with PANDA2.

integral number of plies. Therefore, as a minimum weight is approached, as is the case, for example, at about iteration 55 and again at iteration 122 (see Fig. 37), all lamina are fixed at thickness equal to an integral number of plies and only the web height and outstanding flange width are allowed to vary from design interaction to iteration. Some judgment is required to decide whether to increase or decrease the arbitrary thicknesses to the appropriate integral ply values. Of course, the integral ply design will be feasible if the user increases the thicknesses of all laminae to values corresponding to the next integer, but the resulting panel may be unnecessarily heavy. Therefore, it is best to use some judgment and reduce the thicknesses of some laminae while increasing those of others.

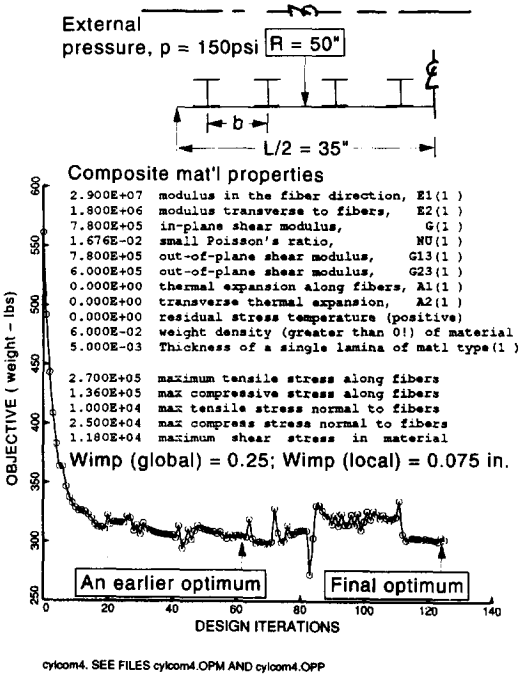

Fig. 37. Objective function (weight) of T-ring stiffened 70-in-long composite cylindrical shell under uniform external hydrostatic pressure, $p = 150$ psi.

During optimization of the composite ring-stiffened cylindrical shell, two optima were found both of which satisfy the integral ply criterion. These two optimum designs are indicated in Figs 37 and 39. The second optimum, labelled "final optimum" in Figs 37 and 39–41 was selected as the configuration for further study with BOSOR4 and STAGS. The optimum design called out in Fig. 36 corresponds to the "final optimum".

In the PANDA2 model the "reduced skin" switch and the "yes tsd" switch were turned on.

BOSOR4 model of the composite panel optimized with PANDA2

Figure 42 is analogous to Fig. 13. However, there are significant differences: the local skin buckling load factor determined by PANDA2 is considerably lower than that predicted for BOSOR4 and STAGS (3.052 vs about 3.9). About half of the difference is caused by the effect of transverse shear deformation (tsd), included in the PANDA2 model, but not in the BOSOR4 or STAGS models. The other half of the difference is caused by the presence of the faying flange, which is ignored in this particular PANDA2 model — an "IQUICK = 1" model (see Ref. [32]) — but included in the BOSOR4 and STAGS models. In

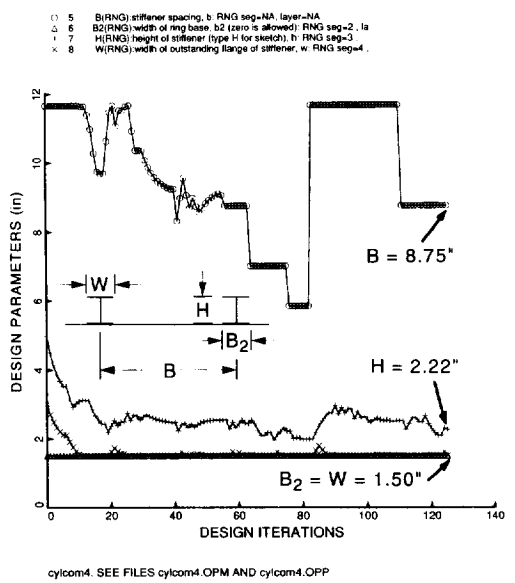

Fig. 38. Evolution of cross-section dimensions of T-ring stiffened 70-in-long composite cylindrical shell under uniform external hydrostatic pressure, $p = 150$ psi.

the composite case BOSOR4 and STAGS predicted general buckling at a slightly higher load factor than PANDA2, whereas the reverse is true for the optimized steel shell. The critical skin buckling mode for the composite shell corresponds in the PANDA2 model to $n = 16$ circumferential halfwaves over the 180° "panel", whereas the critical skin buckling mode for the steel shell corresponds to $n = 20$ halfwaves, even though the ring spacing is the same, $b = 8.75$, in both cases. Finally, according to the BOSOR4 model

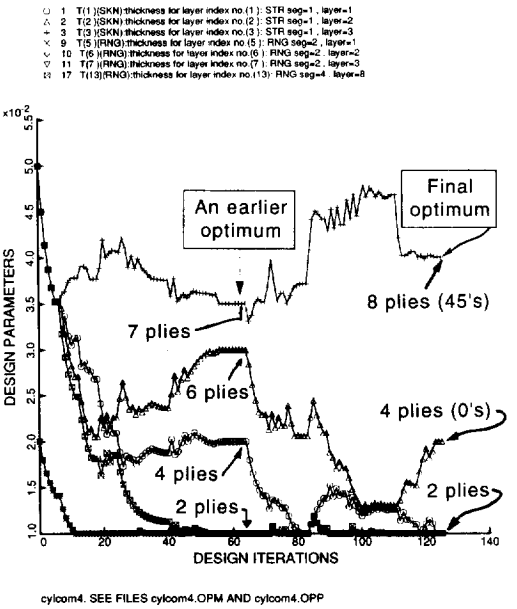

Fig. 39. Evolution of laminae thickness of T-ring stiffened 70-in-long composite cylindrical shell under uniform external hydrostatic pressure, $p = 150$ psi.

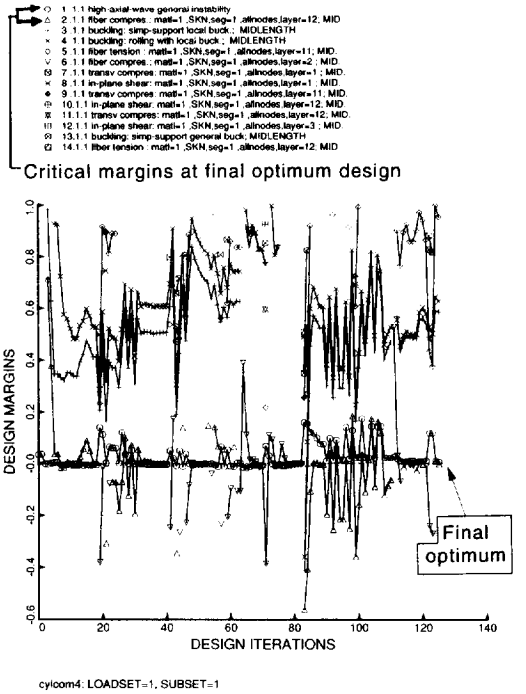

Fig. 40. Margins for the T-ring stiffened 70-in-long hydrostatically compressed composite cylindrical shell corresponding to conditions midway between adjacent rings.

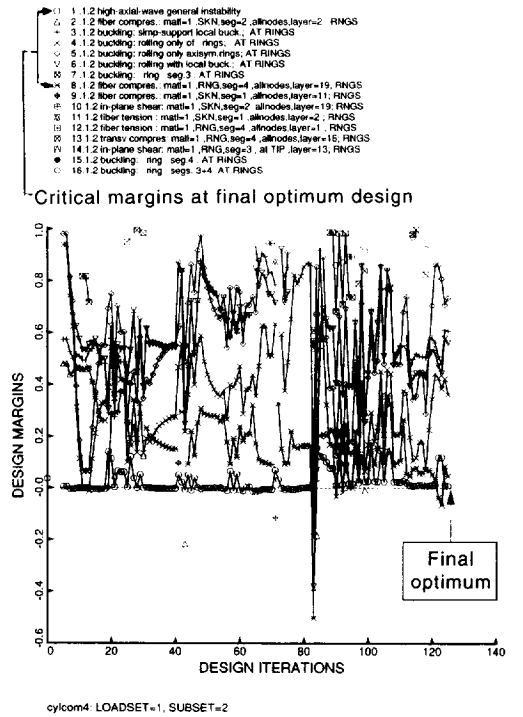

Fig. 41. Margins for the T-ring stiffened 70-in-long hydrostatically compressed composite cylindrical shell corresponding to conditions at a typical ring.

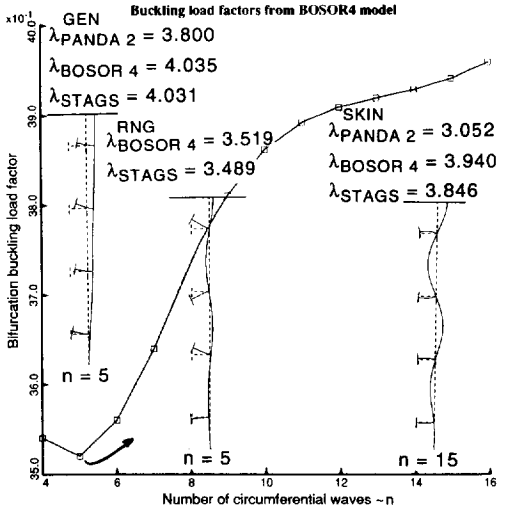

Fig. 42. Buckling mode shapes predicted by BOSOR4 and load factors predicted by PANDA2, BOSOR4, and STAGS for the optimized, perfect 70-in-long hydrostatically compressed composite cylindrical shell.

of the composite shell, there is no clear minimum in the relationship between local skin buckling load factor vs number of circumferential waves (Fig. 42). Instead, there is a flat region in the curve of (buckling load factor) vs n from about $n = 12$ to $n = 16$. There is a true minimum at $n = 5$, but for this relatively low value of n the main characteristic of the buckling mode is ring tripping, as seen from the middle insert in Fig. 42. The curve between $n = 5$ and $n = 16$ in Fig. 42 represents a gradual transition from a mode in which ring tripping predominates to a mode in which skin buckling predominates.

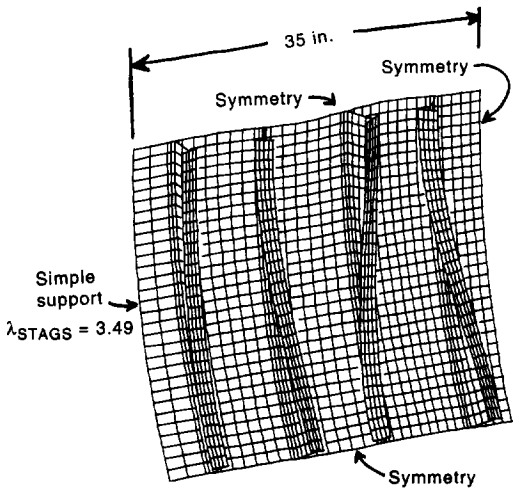

Fig. 43. Ring tripping buckling mode of the T-ring stiffened hydrostatically compressed 70-in-long composite cylindrical shell as predicted by STAGS.

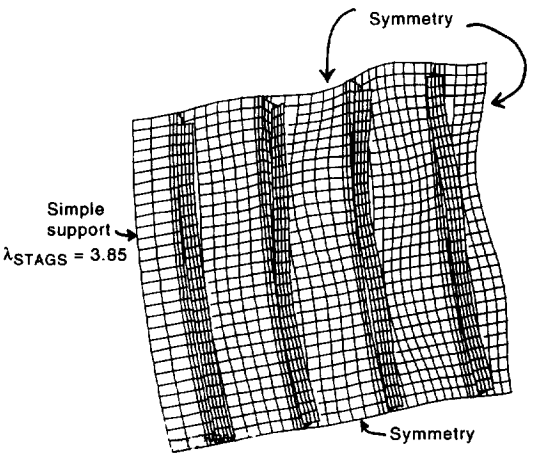

Fig. 44. Local skin buckling mode of the T-ring stiffened hydrostatically compressed 70-in-long composite cylindrical shell as predicted by STAGS.

STAGS model of the composite panel optimized with PANDA2

Figures 43–45 display three buckling modes determined with STAGS. Except for detailed dimensions and material properties, the STAGS model is analogous to that used for the steel shell (see Fig. 14). Again, only 36° of the circumference is included in the STAGS model because the critical general instability buckling mode again has five circumferential waves. Figures 44 and 45, representing the local skin buckling mode and the general instability mode, are analogous to Figs 14 and 16 for the steel shell. Figure 43, the critical buckling mode of the perfect shell in this case, corresponds to ring tripping. It is essentially the same buckling mode as that predicted by BOSOR4 and displayed in the middle insert in Fig. 42. The buckling modes depicted in Figs 44 and 45 are used, with amplitudes set to 0.25 in and 0.075 in, respectively, as imperfection components in the STAGS nonlinear collapse run.

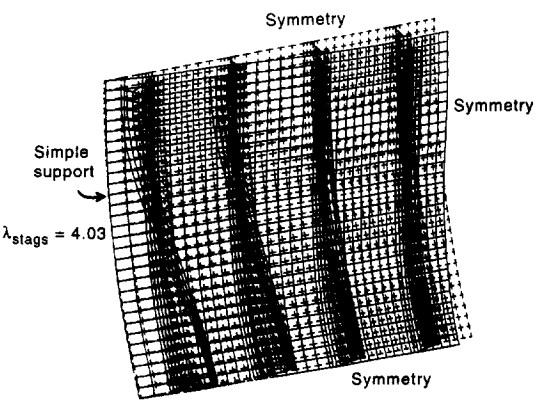

Fig. 45. General buckling mode of the T-ring stiffened hydrostatically compressed 70-in-long composite cylindrical shell as predicted by STAGS.

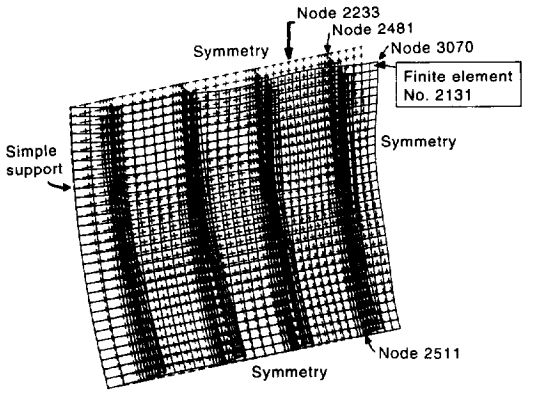

Fig. 46. Deformation of the imperfect composite shell at the design load, $PA = 1.0$, that is, at pressure $p = 150$ psi.

Results from the STAGS nonlinear collapse run are displayed in Figs 46–51. Figure 46 is analogous to Fig. 17 for the steel shell, and Figs 47–50 are analogous to Figs 20–23 for the steel shell. Comparison of Fig. 46 with Fig. 18 reveals that for the composite shell there is much less local skin deformation at the design load, $PA = 1.0$, than is the case for the steel shell. This is partly because of the neglect of the transverse shear deformation (tsd) effect in the STAGS model, partly because of the neglect of the faying flange in the local buckling analysis section of the PANDA2 calculations, and partly due to the use of "reduced skin" in the PANDA2 model. All three differences in the models cause there to be more local skin bending in the PANDA2 model than in the STAGS model: the tsd effect causes the load factor for skin buckling to be lower, which results in more

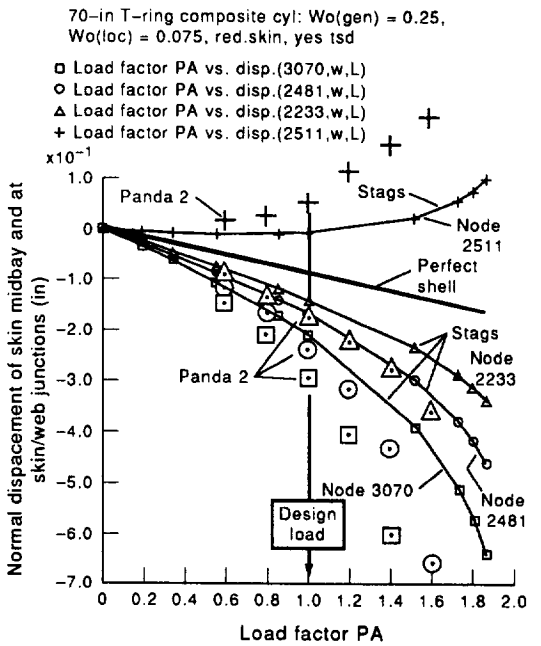

Fig. 47. Comparison of STAGS and PANDA2 predictions of normal displacement for the composite shell.

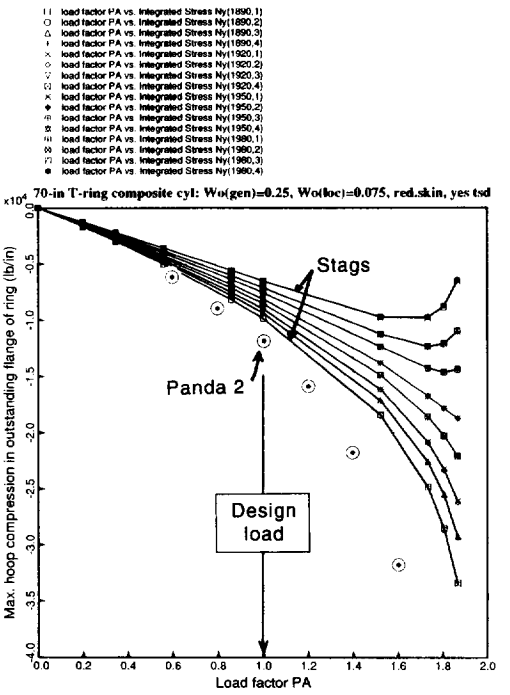

Fig. 48. Comparison of STAGS and PANDA2 predictions of hoop compression Ny in the ring flange of the composite shell where the flange is compressed more than the skin.

amplification of the local buckling modal imperfection at the design load in the PANDA2 model than in the STAGS model; neglect of the faying flange in

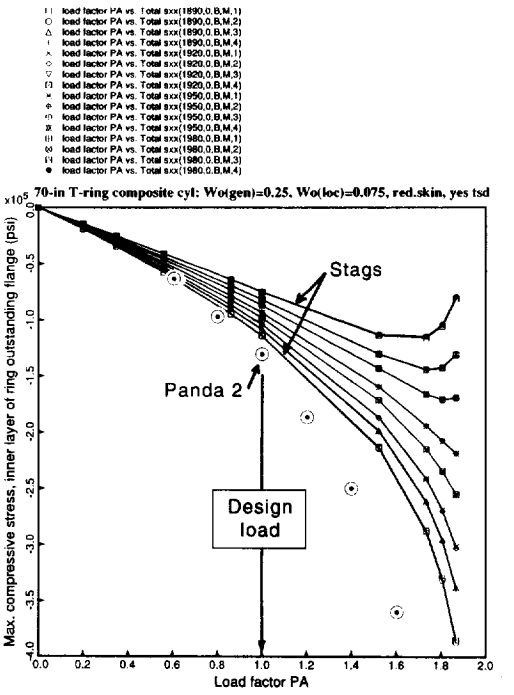

Fig. 49. Comparison of STAGS and PANDA2 predictions of fiber stress in the innermost layer of the ring flange of the composite shell where the flange is compressed more than the skin.

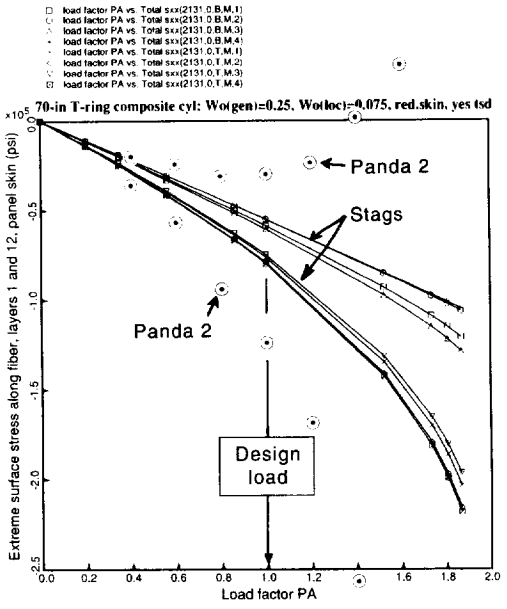

Fig. 50. Comparison of STAGS and PANDA2 predictions of fiber stress in the panel skin of the composite shell where the skin is compressed more than the outstanding flange of the ring. Layers 1 and 12 are the inner and outer layers in Laminate no. 1 (See Fig. 36).

the PANDA2 model further lowers the local buckling load factor, resulting in further amplification of the local modal imperfection; use of "reduced skin" in the PANDA2 model of general buckling of the imperfect shell leads to more overall bending in the PANDA2 model than in the STAGS model, which causes the skin to be locally compressed more in regions where the overall bending is inward. Therefore, in the PANDA2 model the extreme surfaces of the skin are stressed more highly by local bending than is the case in the STAGS model.

Comparison of results from PANDA2 and STAGS

Figures 47–50 pertain to this section. The PANDA2 model displays more overall bending and more local skin bending than the STAGS model (for the reasons listed in the previous paragraph). The PANDA2 model exhibits far more outward displacement than does the STAGS model ("plus" markers in Fig. 47) because of the simplified nature of the PANDA2 analysis: emphasis in the PANDA2 model is put on the most critical behavior, not on accuracy in all details. As in the case of the steel shell, in each of Figs 48 and 49 there is only one curve corresponding to the PANDA2 model, whereas there are many corresponding to the STAGS model. The PANDA2 predictions err on the conservative side.

Figure 50 shows a rather dramatic difference between the predictions of STAGS and PANDA2 for bending stress in the panel skin at finite element no. 2131 (see Fig. 46 for location). The significant difference is caused by there being more amplification of the local buckling mode in the PANDA2 model than in the STAGS model for the reasons given above.

Figure 51 is analogous to Fig. 25 for the steel shell. Ultimate collapse is again caused by ring tripping. In the case of the composite shell ultimate collapse occurs at a significantly higher load factor ($PA = 1.95$) than is the case for the steel shell ($PA = 1.39$ in Fig. 25).

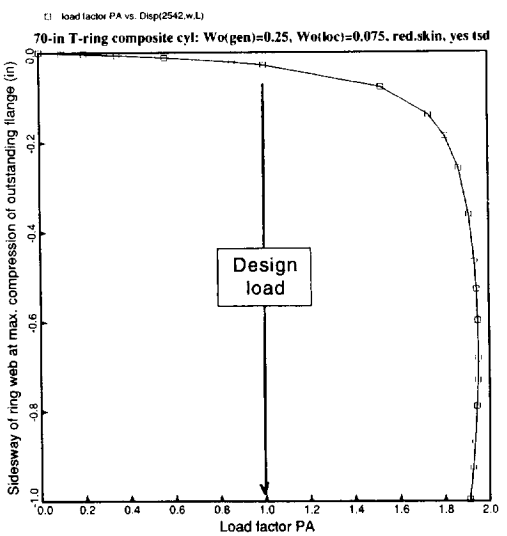

Fig. 51. Ring tripping in the imperfect composite shell designed by PANDA2 with the "reduced skin" and "tsd" switches turned on.

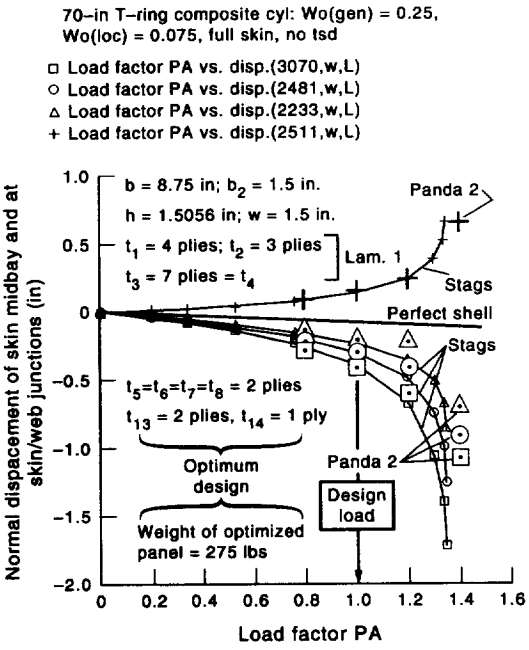

Fig. 52. The optimum design obtained from PANDA2 with the "reduced skin" and "tsd" switches turned off. Comparison of STAGS and PANDA2 predictions of normal displacement for the optimized composite shell.

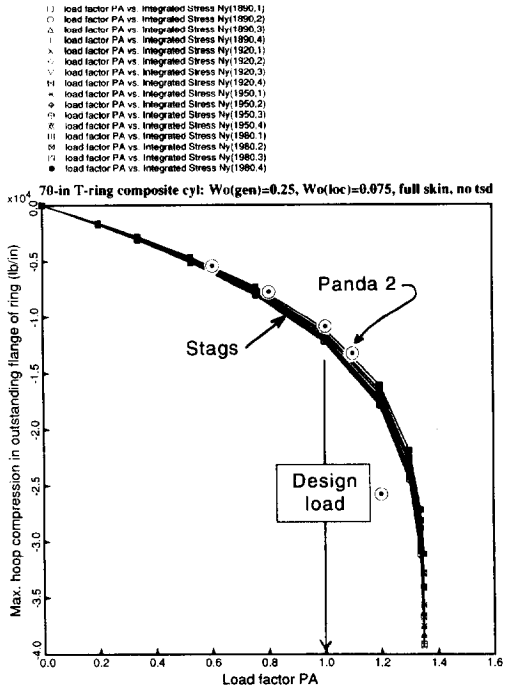

Fig. 53. Comparison of STAGS and PANDA2 predictions of hoop compression Ny in the ring flange of the composite shell where the flange is compressed more than the skin in the design derived by PANDA2 with the "reduced skin" and "tsd" switches turned off.

A less conservative PANDA2 model: "reduced skin" and "tsd" turned off during PANDA2 optimization

Figures 52–56, which are analogous to Figs 47–51, give comparisons between PANDA2 and STAGS predictions for a panel optimized with the "reduced skin" and "tsd" switches turned off. The dimensions and weight of the re-optimized panel appear in Fig. 52. Whereas the weight of the optimized composite panel with the "reduced skin' and "tsd" switches on is 302 lbs, the new panel weighs less: 275 lbs. In this case it appears to be safe to turn off the "reduced skin" switch because the PANDA2 predictions of maximum stress at the design load, $PA = 1.0$, are either conservative with respect to the STAGS predictions (Fig. 55) or very close to the STAGS predictions (Fig. 54) at the design load factor, $PA = 1.0$. By comparing Figs 50 and 55, notice that the STAGS model shows more bending in the panel skin in the latter case. There is still less local skin bending in the STAGS model than in the PANDA2 model because of the different treatment of the faying flanges of the rings in the two models.

Note that one cannot conclude from the results just given that it is safe to ignore the transverse shear deformation (tsd) effect. In all of the STAGS models presented here tsd is ignored. In that respect the PANDA2 results with the "tsd" switch turned on are more reliable than those of STAGS.

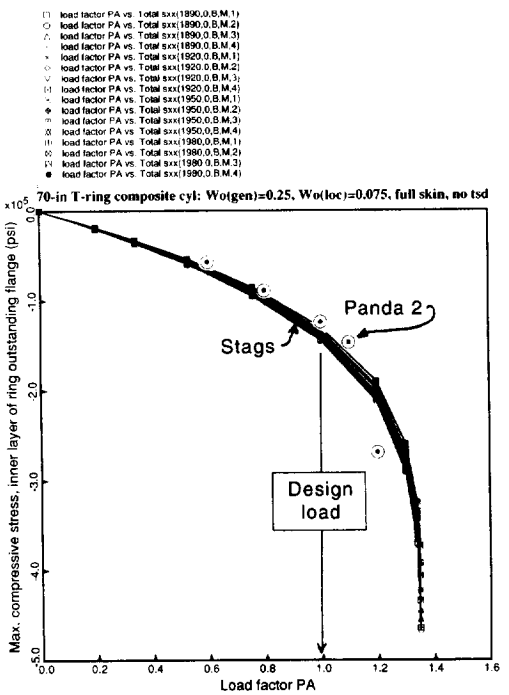

Fig. 54. Comparison of STAGS and PANDA2 predictions of fiber stress in the innermost layer of the ring flange of the composite shell where the flange is compressed more than the skin. Shell designed with "reduced skin" and "tsd" switches turned off.

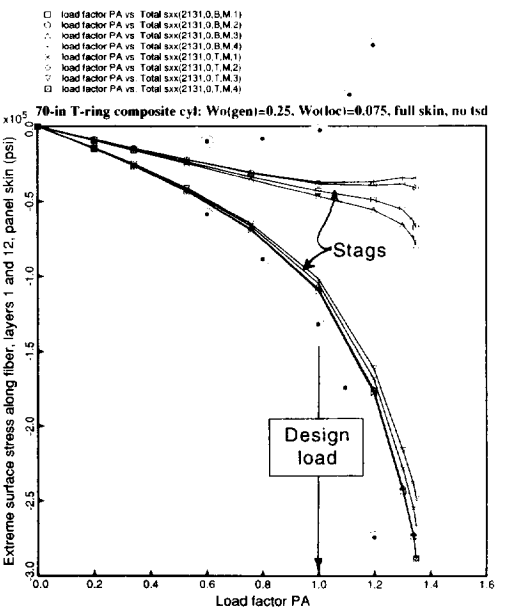

Fig. 55. Comparison of STAGS and PANDA2 predictions of fiber stress in the panel skin of the composite shell where the skin is compressed more than the outstanding flange of the ring. Shell designed with "reduced skin" and "tsd" switches turned off.

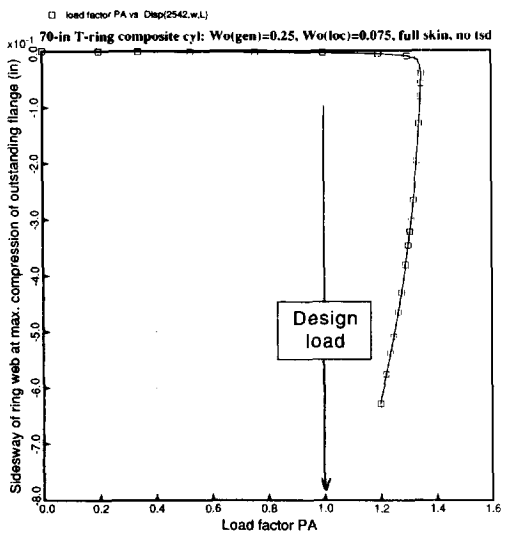

Fig. 56. Ring tripping in the imperfect composite shell designed by PANDA2 with the "reduced skin" and "tsd" switches turned off.

EXAMPLE 4: OPTIMUM DESIGN OF AN IMPERFECT HYDROSTATICALLY COMPRESSED T-RING-STIFFENED COMPOSITE CYLINDRICAL SHELL 200 INCHES LONG

Figures 57–70 pertain to this section.

The results presented in this section are analogous to those presented for the 70-in-long composite ring-stiffened cylindrical shell. The radius of the shell is the same, $R = 50$ in, and the design pressure is still $p = 150$ psi. The overall arrangement of the layers and material properties are the same as depicted in Figs 36 and 37, although the optimum design is different, of course. The same imperfection amplitudes are used here, Wimp(global) = 0.25 in and Wimp(local) = 0.075 in. Again, the PANDA2 model is a panel which spans 180° of the circumference.

According to PANDA2, the optimized panel, if perfect, buckles in the general instability mode at a load factor of 2.59 with three halfwaves over the 180° of the circumference, and in the local skin buckling mode at a load factor of 2.34 with 16 halfwaves over the 180°. A BOSOR4 model yields a ciritical general instability load factor of 2.70 and a local buckling load factor of about 2.98, although, as is the case for the 70-in-long composite cylinder, there is no clear minimum skin buckling load factor as a function of number of circumferential waves: the behavior is similar to that displayed in Fig. 42 for the 70-in-long composite shell.

It is more difficult to compare with STAGS in this case because a much larger piece of structure must be discretized in the STAGS model, since the shell is longer while the ring spacing is about the same. Because the shell is longer, the critical general buckling mode has fewer circumferential waves than is the case for the 70-in-long composite panel. Therefore, a larger circumferential sector of the shell must be included in the STAGS model.

The optimum design obtained by PANDA2 is listed in Fig. 61. The general instability mode has three circumferential halfwaves over the 180° circumference of the shell. Therefore, the STAGS model must include at least 60° of the circumference. In order to make the STAGS analysis more tractable, a compound model was set up in which the rings were "smeared" over the largest portion of the structure, as indicated in Fig. 57.

Figures 57–59 are analogous to Figs 14–16 for the ring-stiffened steel cylindrical shell. Figures 57 and 58 display two views of the local buckling mode

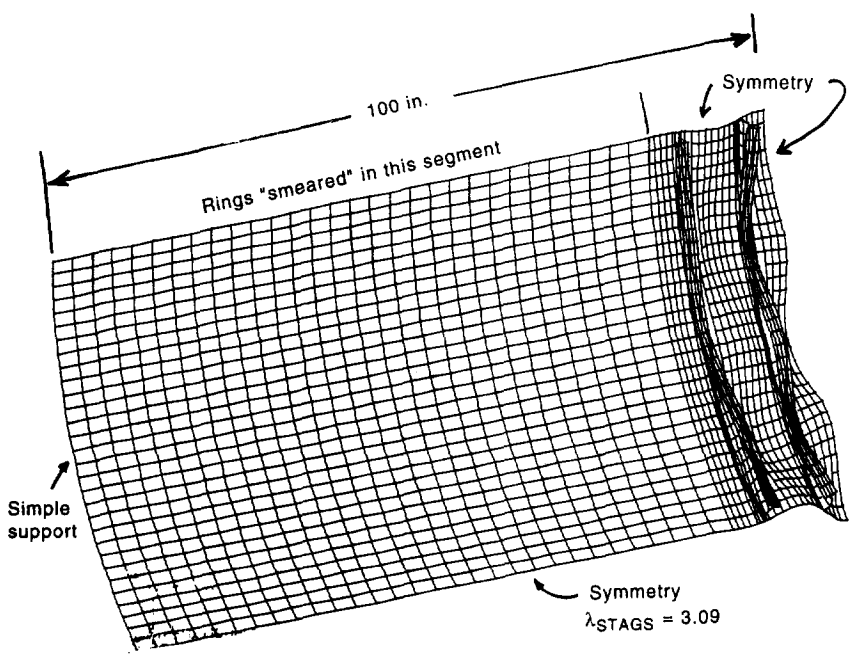

Fig. 57. Local skin buckling mode of the T-ring stiffened hydrostatically compressed 200-in-long composite cylindrical shell as predicted by STAGS.

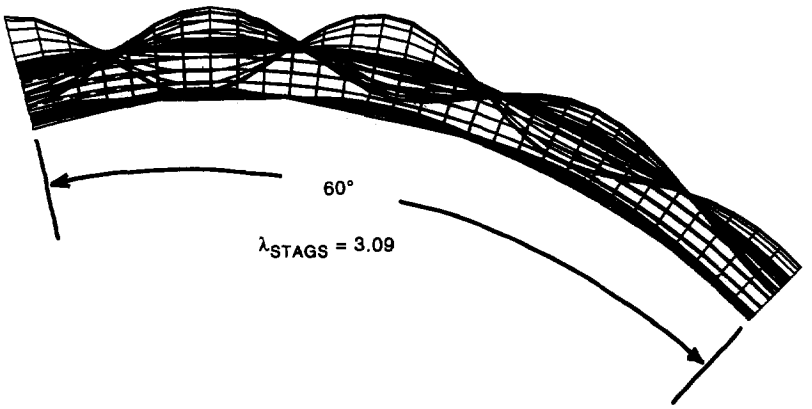

Fig. 58. Another view of local buckling mode shown in the previous figure.

predicted with STAGS. Note from Fig. 58 that, unlike the example of the steel shell (Fig. 15), the amplitude of the local mode is nonuniform in the circumferential direction. This nonuniformity probably represents the superposition of two eigenvectors from very closely spaced eigenvalues. It does not present a serious problem, however. The signs of the amplitudes of the two buckling modal imperfections, general and local, must be chosen with care so that the maximum amplitude of the local imperfection occurs where the general modal imperfection causes the shell to bend inward and compress the skin the most. Figure 59 shows the general buckling mode predicted with the STAGS model.

Figures 60–65 contain the results from the STAGS nonlinear collapse analysis. Figure 60 shows the deformed shell at the design load, $PA = 1.0$, that is, at the external pressure, $p = 150$ psi. As is the case with the 70-in-long composite cylinder, there is much less local bending at the design load in this example than there is for the optimized steel ring-stiffened shell (Fig. 18).

There is a source of possible nonconservativeness in the STAGS model: only two rings are represented as flexible branched structures, while the rings are smeared out over the remainder of the shell. A better model would have three or four of the rings represented as flexible segments rather than just two.

Figures 61–65 are analogous to Figs 47–51 for the 70-in-long composite cylindrical shell. Although the PANDA2 model exhibits more overall and local bending than the STAGS model, as is evident from Fig. 61, the maximum hoop stress in the outstanding flange of the ring at the design load, $PA = 1.0$ (Fig. 63), is slightly more in the STAGS model than in the PANDA2 model. The difference is caused by the twisting of the ring in the STAGS model, which is not accounted for in the PANDA2 (IQUICK = 1) model, as has already been mentioned. This twisting

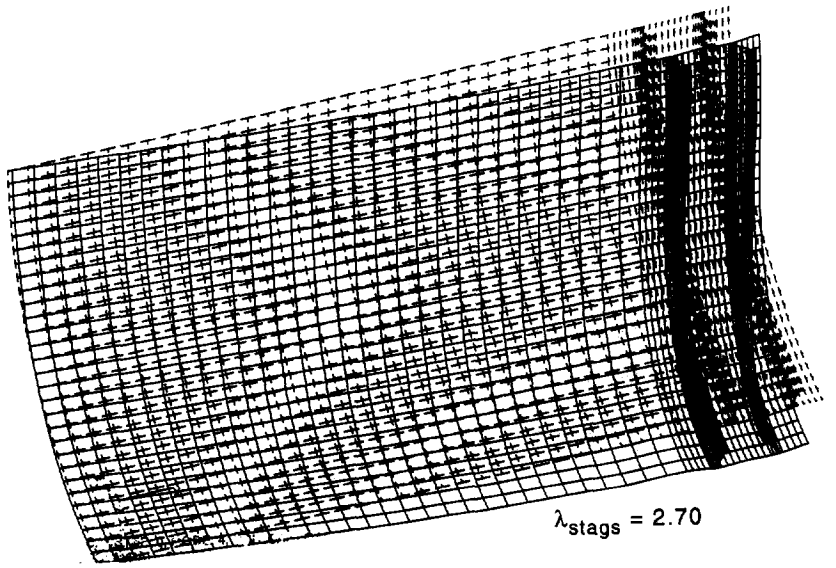

Fig. 59. General buckling mode of the T-ring stiffened hydrostatically compressed 200-in-long composite cylindrical shell as predicted by STAGS.

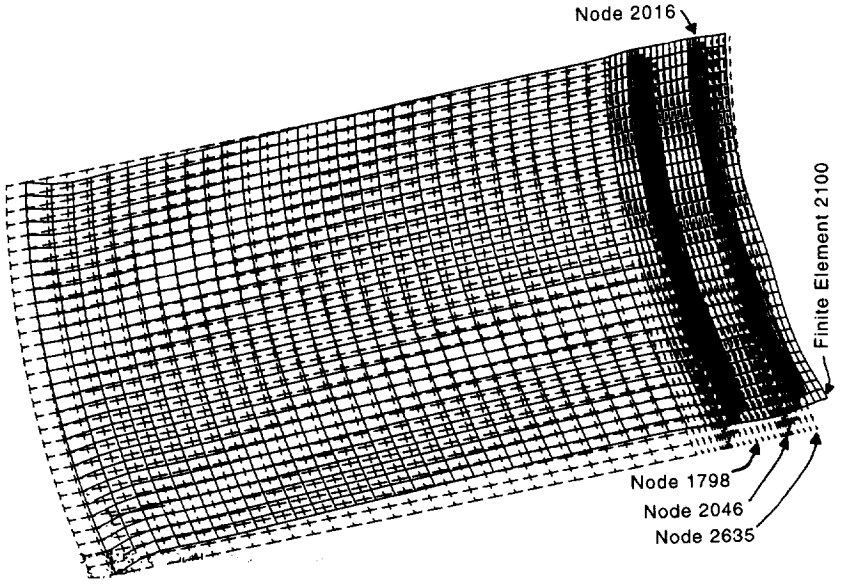

Fig. 60. Deformation of the imperfect composite shell at the design load, $PA = 1.0$, that is, at pressure $p = 150$ psi.

causes the hoop stresses to be nonuniform over the width of the outstanding flange in the STAGS model. Figure 65 demonstrates that ultimate collapse of the shell is caused by ring tripping, as has been the case for most of these examples.

"Reduced skin" and "tsd" switches turned off in PANDA2

Figures 66–70 are analogous to Figs 52–56 for the 70-in-long composite shell. The 200-in-long composite shell is re-optimized with the "reduced skin" and "tsd" switches turned off in the PANDA2 analysis, and comparisons are made with results from a STAGS model of the re-optimized shell. The weight of the panel is reduced from 801 lbs to 769 lbs. There is generally better agreement between PANDA2 and STAGS for this case than for the case with the "reduced skin" and "tsd" switches on in the

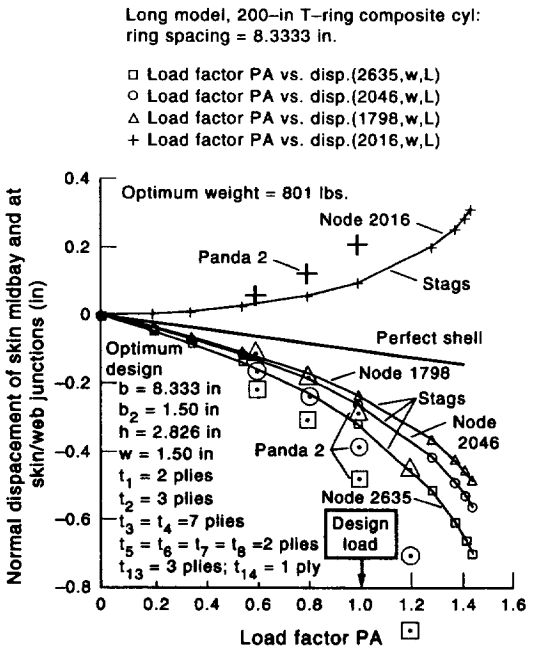

Fig. 61. Optimum design obtained by PANDA2 with the "reduced skin" and "tsd" switches turned on. Comparison of STAGS and PANDA2 predictions of normal displacement for the composite shell.

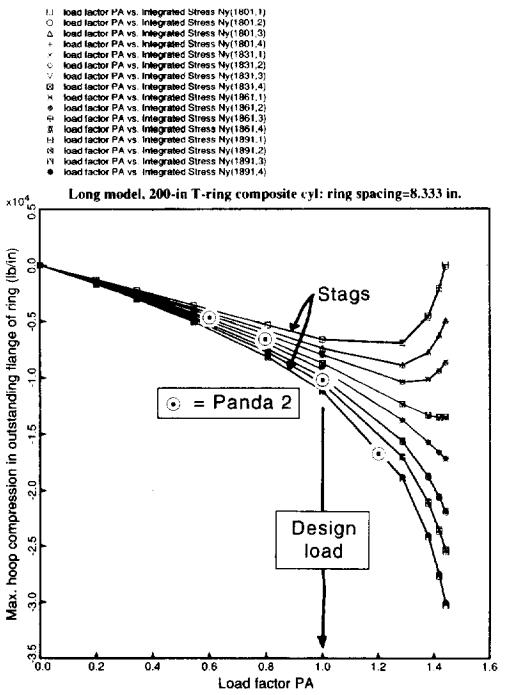

Fig. 62. Comparison of STAGS and PANDA2 predictions of hoop compression Ny in the ring flange of the composite shell where the flange is compressed more than the skin. "Reduced skin" and "tsd" switches turned on.

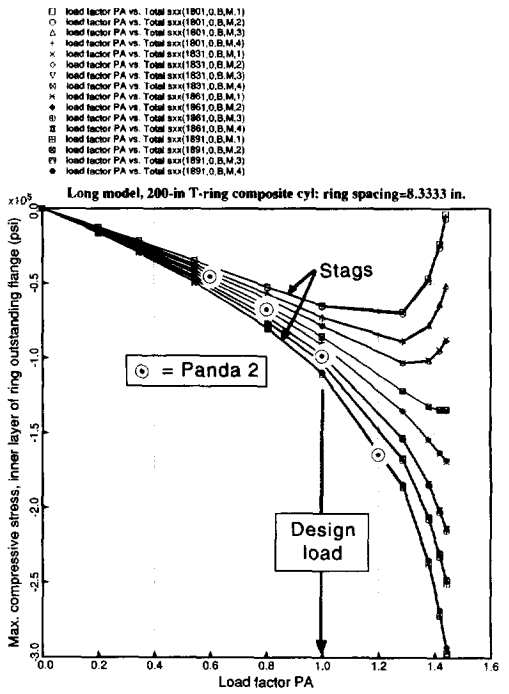

Fig. 63. Comparison of STAGS and PANDA2 predictions of fiber stress in the innermost layer of the ring flange of the composite shell where the flange is compressed more than the skin. "Reduced skin" and "tsd" swtiches turned on.

PANDA2 analysis. However, for some unknown reason, the new STAGS model displays even less local bending (compare Fig. 69 with Fig. 64). The ultimate collapse load of the shell is reduced from a

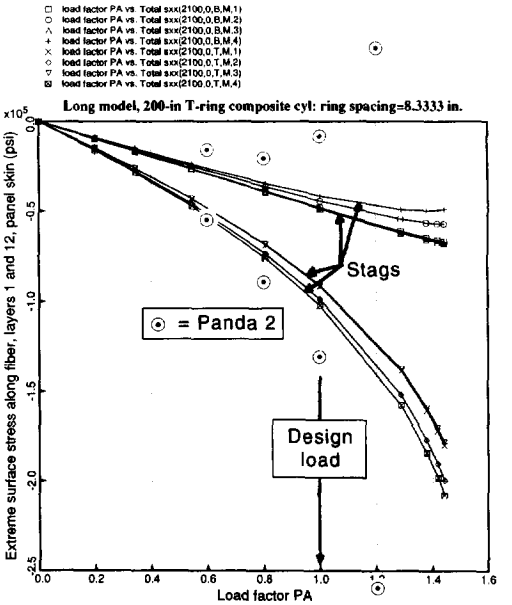

Fig. 64. Comparison of STAGS and PANDA2 predictions of fiber stress in the panel skin of the composite shell where the skin is compressed more than the outstanding flange of the ring. "Reduced skin" and "tsd" switches turned on.

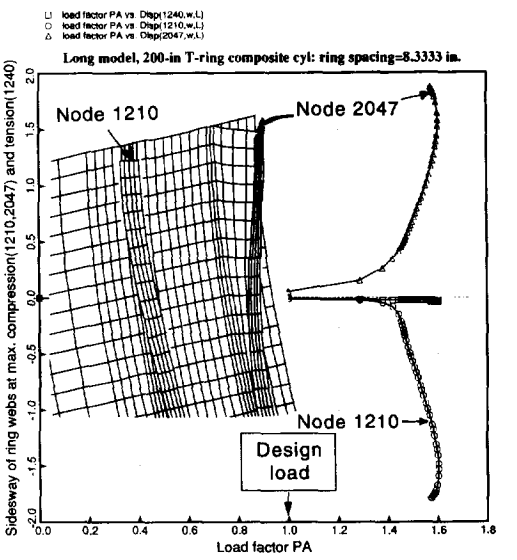

Fig. 65. Ring tripping in the imperfect composite shell designed by PANDA2 with the "reduced skin" and "tsd" switches turned on.

load factor of 1.6 (Fig. 65) to a load factor of 1.43 (Fig. 70).

Again, note that the transverse shear deformation (tsd) effect is neglected in both the STAGS and PANDA2 models used to generate the data in Figs 66–70. Therefore, although the results from PANDA2 (with "reduced skin" and "tsd" turned off) and STAGS agree reasonably well, and although the maximum compressive stress along the fibers predicted by STAGS is below the allowable value of

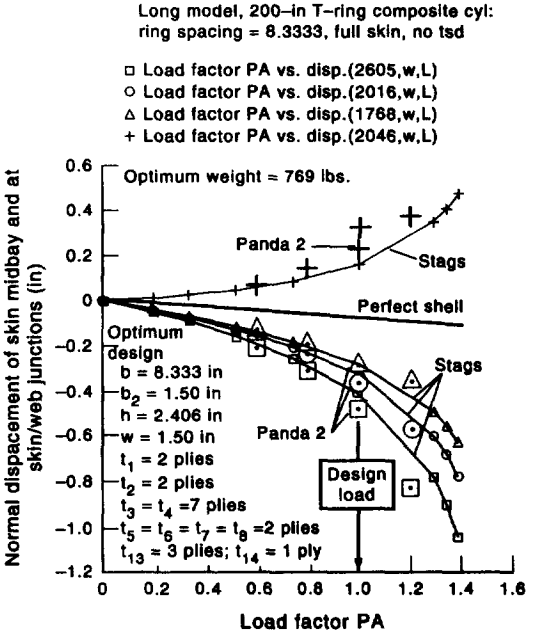

Fig. 66. The optimum design obtained from PANDA2 with the "reduced skin" and "tsd" switches turned off. Comparison of STAGS and PANDA2 predictions of normal displacement for the optimized composite shell.

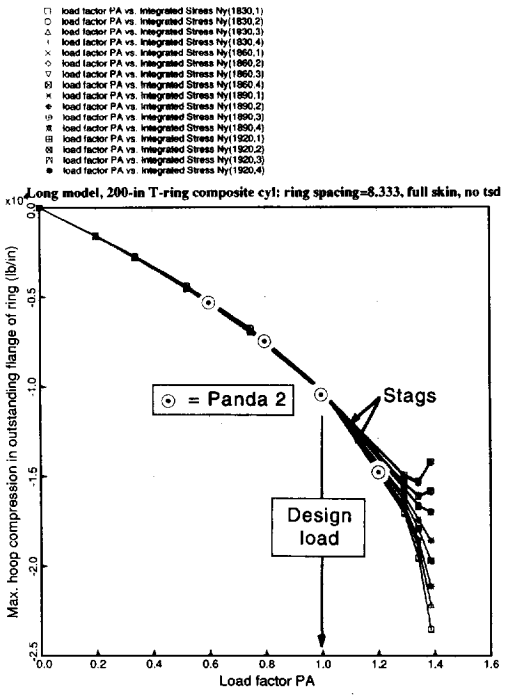

Fig. 67. Comparison of STAGS and PANDA2 predictions of hoop compression Ny in the ring flange of the composite shell where the flange is compressed more than the skin in the design derived by PANDA2 with the "reduced skin" and "tsd" switches turned off.

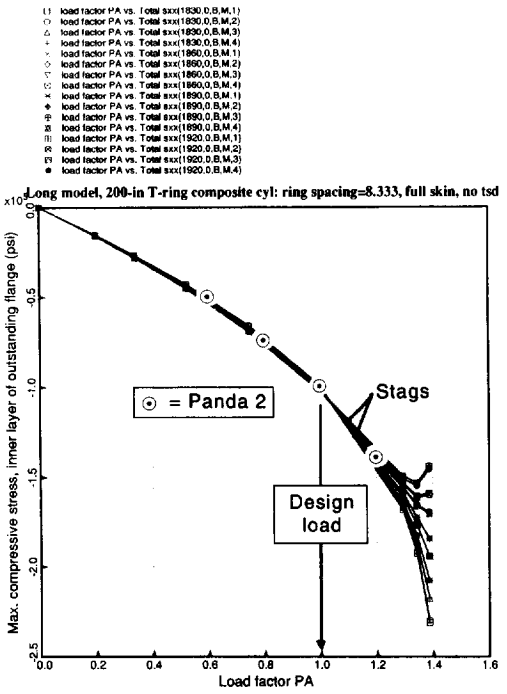

Fig. 68. Comparison of STAGS and PANDA2 predictions of fiber stress in the innermost layer of the ring flange of the composite shell where the flange is compressed more than the skin. Shell designed with "reduced skin" and "tsd" switches turned off.

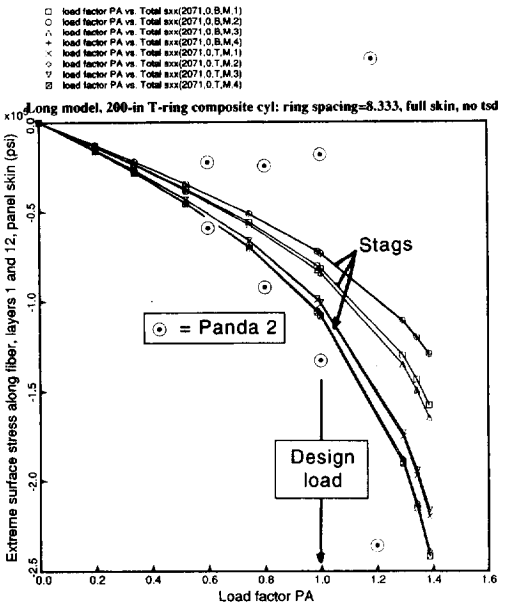

Fig. 69. Comparison of STAGS and PANDA2 predictions of fiber stress in the panel skin of the composite shell where the skin is compressed more than the outstanding flange of the ring. Shell designed with "reduced skin" and "tsd" switches turned off.

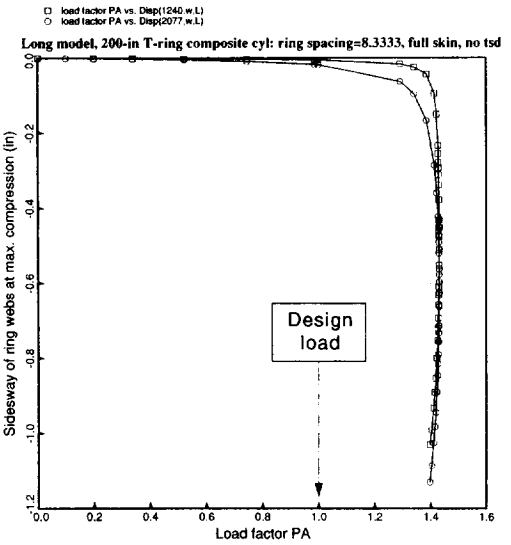

Fig. 70. Ring tripping in the imperfect composite shell designed by PANDA2 with the "reduced skin" and "tsd" switches turned off.

136 ksi (see the list of allowable stresses in Fig. 37), the optimum design generated by PANDA2 with "reduced skin" and "tsd" turned off may be unsafe. It is recommended that users always generate optimum designs with the "reduced skin" and "tsd" switches on.

CONCLUSIONS

In designing shell structures subjected to destabilizing loads, one is constantly faced with the question,

"What knockdown factors should I use?" One of the main objectives of the work summarized in this paper has been to produce a design tool for which this question is unnecessary. The PANDA2 user must still provide appropriate amplitudes of local, inter-ring, and general buckling modal imperfections. However, approximate values of these amplitudes can be more easily supplied because, unlike knock-down factors, they are physically related to the tolerances to which a panel is to be fabricated.

The results given here appear to qualify PANDA2 for the preliminary design of stiffened cylindrical panels with both overall and local buckling modal initial imperfections. Of course, only a limited number of cases are given in which PANDA2 and STAGS results are compared. All of these cases involve hydrostatically compressed cylindrical shells with internal T-shaped rings (the submarine pressure hull design problem). In previous papers, PANDA2 and STAGS predictions for axially stiffened curved [37] and flat [31, 37] panels under combined loads are discussed. A much wider spectrum of problems should be explored with both PANDA2 and STAGS, including stiffened cylindrical panels with combined axial compression, in-plane shear, and internal pressure (the aircraft fuselage design problem).

The following overall conclusions might be drawn from the results presented here:

(1) PANDA2 predictions generally (but not always!) err on the conservative side. The optimum designs produced by PANDA2 do not appear to be overly conservative.

(2) A frequently used "classical" method for accounting for initial imperfections in the design of stiffened panels is unsafe. It is NOT recommended that the applied load be "knocked up" by a generally accepted knockdown factor as follows

(applied load) =

(ultimate load)/(knockdown factor)

and optimum designs be obtained for perfect panels subjected to the higher applied load, since the resulting optimum design may well display early failure in tests or in numerical experiments in which imperfections of reasonable amplitude are explicitly included in the formulation.

(3) In all of the T-ring stiffened cylindrical shells designed by PANDA2 with the local and general buckling modal imperfections included explicitly in the model, ultimate collapse of the imperfect optimized shell, according to STAGS, is by ring tripping. Although this ultimate collapse occurs at a load factor well above $PA = 1.0$ (the design load) in every case, it may yet be a good idea further to modify the PANDA2 code by increasing the factor of safety for ring tripping (presently set internally at 1.6) to a value of 1.8 or even 2.0. In this way the optimum designs will have outstanding flanges of greater width. It is likely that the optimum weight will not increase a significant amount as a result of this modification.

(4) It may be necessary to use the "reduced skin stiffness" option in PANDA2 when generating optimum designs. This question should be addressed through additional cases.

(5) Comparisons between STAGS and PANDA2 with the use of STAGS models in which the effect of transverse shear deformation (tsd) is included should be obtained. In all of the STAGS models presented here, tsd effects were neglected.

(6) The PANDA2 models for the ring-stiffened cylindrical shells without stringers are all of the closed form "PANDA-type" (Bushnell [34] IQUICK = 1). At present there is no IQUICK = 0 capability, that is, no capability of modeling via PANDA2 the skin-ring module as a discretized entity in a manner analogous to the discretized skin stringer module described in previous papers on PANDA2 [32]. Local buckling of the skin between rings is predicted based on the assumption that the rings offer no elastic support nor do they "encourage" the skin to buckle via torsion-bending buckling. Local buckling is predicted as if the skin were simply supported along the line of intersection between ring web and panel skin. Ring rolling and skin buckling are treated as separate phenomena, not coupled as is the case with the IQUICK = 0 (discretized) skin-stringer module model. Consequently, the effect of ring faying flanges is ignored in the PANDA2 model. This may on occasion lead to overly conservative optimum designs.

(7) The destabilizing effect of axisymmetric bands of hoop compression induced by axial waviness in an imperfection pattern that is amplified by axial compression (this effect is dominant in Koiter's special theory [45]) was NOT included in the 1994 PANDA2 formulation used here. The effect of reduced circumferential curvature in the inward circumferential lobes of the imperfection pattern was included, however. In PANDA2, buckling load factors of imperfect panels are computed as if the minimum local circumferential curvature exists everywhere in the panel. This is a conservative assumption, and seems to compensate for the lack of conservatism inherent in the neglect of the induced local hoop compression. See Ref. [35] for recent updates.

Acknowledgements—The senior author wishes to express his appreciation for the continuing support of Mr Stan Simson and Mr Dan Trites, Stress and Fractural Mechanics Department in Lockheed Missiles and Space Company's satellite Systems Division.

The authors are indeed grateful to Frank Brogan and Charles Rankin, the developers of STAGS, for their contributions to the creation of the STAGS postprocesor STAGSPP, for their quick responses to request for modifications in STAGS, and for their patience in teaching the senior author how to use STAGS. The authors also wish to thank Harold Cabiness for his contribution to the creation of STAGSPP, which generates figures such as Figs 20–23.

REFERENCES

1. D. Bushnell and W. D. Bushnell, Minimum-weight design of a stiffened panel via PANDA2 and evaluation of the optimized panel via STAGS. *Comput. Struct.* **50,** 569–602 (1994).
2. R. Le Riche and R. T. Haftka, Optimization of laminate stacking sequence for buckling load maximization by genetic algorithm. AIAA paper 92-2314-CP, *Proc. 33rd AIAA Structures, Structural Dynamics, and Materials Conf.*, Part 5, pp. 2564–2575.
3. M. Lombardi, R. T. Haftka and C. Cinquini, Optimization of composite plates for buckling by simulated annealing. AIAA paper 92-2313-CP, *Proc. 33rd AIAA Structures, Structural Dynamics and Materials Conf.*, Part 5, pp. 2552–2563 (1992).
4. S. Nagendra, R. T. Haftka and Z. Gürdal, Stacking sequence optimization of simply supported laminates with stability and strain constraints. AIAA paper 92-2310-CP, *Proc. 33rd AIAA Structures, Structural Dynamics, and Materials Conf.*, Part 5, pp. 2526–2535 (1992).
5. R. T. Haftka and J. L. Walsh, Stacking sequence optimization for buckling of laminated plates by integer programming. AIAA paper 91-0970-CP, *Proc. 32nd AIAA Structures, Structural Dynamics, and Materials Conf.*, Part 1, pp. 267–274 (1991).
6. L. Librescu and M. A. Souza, Postbuckling of geometrically imperfect shear-deformable flat panels under combined thermal and compressive edge loadings. *J. Appl. Mech.* **60,** 526–534 (1993).
7. C. Collier, Structural analysis and sizing of stiffened, metal matrix composite panels for hypersonic vehicles. In: *Proc. AIAA Fourth Int. Aerospace Planes Conf.*, 1–4 December, Orlando, FL (1992).
8. W. L. Ko and R. H. Jackson, Combined compressive and shear buckling analysis of hypersonic aircraft sandwich panels. AIAA paper 92-2487-CP, *Proc. 33rd AIAA Structures, Structural Dynamics, and Materials Conf.*, Part 5, pp. 3198–3225 (1992).
9. C. A. Meyers and M. W. Hyer, Thermally-induced, geometrically nonlinear response of symmetrically laminated composite plates. AIAA paper 92-2539-CP, *Proc. 33rd AIAA Structure, Structural Dynamics, and Materials Conf.*, Part 2, pp. 1027–1037 (1992).
10. A. K. Noor, J. H. Starnes Jr and J. M. Peters, Thermomechanical buckling and postbuckling of multilayered composite panels. AIAA paper 92-2541-CP, *Proc. 33rd AIAA Structures, Structural Dynamics, and Materials Conf.*, Part 2, pp. 1052–1068 (1992).
11. K. Chandrashekhara, Thermal buckling of anisotropic laminated cylindrically curved panels. AIAA paper 91-0915-CP, *Proc. 32nd AIAA Structures, Structural Dynamics, and Materials Conf.*, Part 2, pp. 933–937 (1991).
12. M. S. Anderson and D. Kennedy, Inclusion of transverse shear deformation in exact buckling and vibration analysis of composite plate assemblies. AIAA paper 92-2287-CP, *Proc. 33nd AIAA Structures, Structural Dynamics, and Materials Conf.*, Part 1, pp. 283–291 (1992).
13. J.-P. Jeusette and G. Laschet, Pre- and postbuckling finite element analysis of curved composite and sandwich panels. *AIAA J.* **28,** 1233–1239 (1990).
14. L. Librescu and M. A. Souza, Postbuckling behavior of shear deformable flat panels under the complex action of thermal and in-plane mechanical loadings. AIAA paper 91-0913-CP, *Proc. 32nd AIAA Structures, Structural Dynamics, and Materials Conf.*, Part 2, pp. 917–925 (1991).
15. L. Librescu and M. Stein, A geometrically nonlinear theory of transversely isotropic laminated composite plates and its use in the post-buckling analysis. *Thin-Walled Struct.*, **11,** 177–01 (1991).
16. L. Librescu and M.-Y. Chang, Effects of geometric imperfections on vibration of compressed shear deformable laminated composite curved panels. *Acta Mech.* **96,** 203–224 (1993).
17. R. C. Averill and J. N. Reedy, Thermomechanical postbuckling analysis of laminated composite shells. AIAA paper 93-1337-CP, *Proc. 34th AIAA Structures, Structural Dynamics, and Materials Conf.*, Part 1, pp. 351–360 (1993).
18. A. Tabiei and G. J. Simitses, Buckling of moderately thick, laminated cylindrical shells under torsion. AIAA paper 93-1334-CP, *Proc. 34th AIAA Structures, Structural Dynamics, and Materials Conf.*, Part 1, pp. 315–325 (1993).
19. M. P. Nemeth, Buckling behavior of long symmetrically laminated plates subjected to compresion, shear, and inplane bending loads. AIAA paper 92-2286-CP, *Proc. 33rd AIAA Structures, Structural Dynamics, and Materials Conf.*, Part 2, pp. 274–282 (1992).
20. S. T. Dennis, B. A. Horban and A. N. Palazotto, Instability in a cylindrical panel subjected to normal pressure. AIAA paper 92-2234-CP, *Proc. 33rd AIAA Structure, Structural Dynamics, and Materials Conf.*, Part 1, pp. 100–108 (1992).
21. S. Fan, B. Kroplin and B. Geier, Buckling, postbuckling, and failure behavior of composite-stiffened panels under axial compression. AIAA paper 92-2285-CP, *Proc. 33rd AIAA Structures, Structural Dynamic, and Materials Conf.*, Part 1, pp. 264–273 (1992).
22. T. Weller and J. Singer, Durability of stiffened composite panels under repeated buckling. *Int. J. Solids Struct.* **26,** 1037-1069 (1990).
23. S. H. Lucas and R. C. Davis, MacPASCO: a Macintosh-based interactive graphic preprocessor for structural analysis and sizing. AIAA paper 91-1208-CP, *Proc. 32nd AIAA Structures, Structural Dynamic, and Materials Conf.*, Part 1, pp. 612–626 (1991).
24. R. P. Ley, E. R. Johnson and Z. Gürdal, Buckling of imperfect, anisotropic, ring-stiffened cylinders under combined loads. AIAA paper 92-2232-CP, *Proc 33rd AIAA Structures, Structural Dynamics, and Materials Conf.*, Part 1, pp. 86–94. *AIAA J.* (in press).
25. R. P. Ley, Z. Gürdal and E. R. Johnson, Optimal design of imperfect anisotropic, ring-stiffened cylinders under combined loads. AIAA paper 93-1526-CP, *Proc. 34th AIAA Structures, Structural Dynamics, and Materials Conf.*, Part 4, pp. 1881–1889, *J. struct. Optim.* (Submitted).
26. L. Librescu, N. K. Chandiramani, M. P. Nemeth and J. H. Jr. Starnes, Postbuckling of laminated flat and curved panels under combined thermal and mechanical loadings. AIAA paper 93-1563-CP, *Proc. 34th AIAA Structures, Structural Dynamics, and Materials Conf.*, pp. 2229–2239 (1993).
27. L. Librescu, W. Lin, M. P. Nemeth and J. H. Jr. Starnes, Classical versus non-classical postbuckling behavior of laminated composite panels under complex loading conditions. In: *Nonclassical Problems of the Theory and Behavior of Structures Exposed to Complete Environmental Conditions* (Edited by L. Librescu), AMD Vol. 164, pp. 169–182 (1993).
28. D. J. Dawe, S. S. E. Lam and Z. G. Azizian, Finite strip post-local-buckling analysis of composite prismatic plate structures. *Comput. Struct.* **48,** 1011–1024 (1993).
29. H.-S. Shen and F. W. Williams, Post-buckling analysis of laminated stiffeners. *Comput. Struct.* **48,** 1117–1124 (1993).
30. J. Arbocz and J. M. A. M. Hol, Shell stability analysis in a computer aided engineering (CAE)

environment. AIAA paper 93-1333-CP, *Proc. 34th AIAA Structures, Structural Dynamics, and Materials Conf.*, Part 1, pp. 300–314 (1993).
31. D. Bushnell and W. D. Bushnell, Optimum design of composite stiffened panels under combined loading. *Comput. Struct.* **55,** 819–856 (1995).
32. D. Bushnell, PANDA2-program for minimum weight design of stiffened, composite, locally buckled panels. *Comp. Struct.* **25,** 469–605 (1987). See also, *Compt. Struct.* **44,** 1091–1119 (1992).
33. D. Bushnell, Use of PANDA2 to optimize composite, imperfect, stiffened, locally buckled panels under combined in-plane loads and normal pressure. *Design and Analysis of Composite Material Vessels*, PVP Vol. 121 (Edited by D. Hui and T. Kozik), pp. 21–42 (1987).
34. D. Bushnell, Theoretical basis of the PANDA computer program for preliminary design of stiffened panels under combined in-plane loads. *Comput. Struct.* **27,** 541–563 (1987).
35. D. Bushnell, PANDA2.NEWS, Unpublished literature distributed with PANDA2.
36. D. Bushnell, Improvements to PANDA2, Vol. 1; Vol. 2, Part 1; Vol. 2, Part 2. Unpublished literature distributed with PANDA2.
37. D. Bushnell, Optimization of composite, stiffened, imperfect panels under combined loads for service in the postbuckling regime. *Comput. Meth. appl. Mech. Engng* **103,** 43–114 (1993).
38. B. O. Almroth and F. A. Brogan, The STAGS computer code. NASA CR-2950, NASA Langley Research Center, Hampton, VA (1978).
39. C. C. Rankin and F. A. Brogan, An element independent corotational procedure for the treatment of large rotations. *J. Pres. Ves. Tech.* **108,** 165–174.
40. G. A. Thurston, F. A. Brogan and P. Stehlin, Postbuckling analysis using a general purpose code. *AIAA J.* **24,** 1013–1020 (1986).
41. C. C. Rankin, P. Stehlin, and F. A. Brogan, Enhancements to the STAGS computer code. NASA CR 4000, NASA Langley Research Center, Hampton, VA (1986).
42. G. N. Vanderplaats and H. Sugimoto, A general-purpose optimization program for engineering design. *Comput. Struct.* **24,** 13–21 (1986).
43. B. O. Almroth, Influence of edge conditions on the stability of axially compressed cylindrical shells. *AIAA J.* **4,** 134–140 (1966).
44. R. M. Jones and J. C. F. Hennemann, Effect of prebuckling deformations on buckling of laminated composite circular cylindrcial shells. *AIAA J.* **18,** 110–115 (1980). [See also, *Proc. AIAA/ASME 19th SDM Conf.* pp. 370–379 (1978).]
45. W. T. Koiter, The effect of axisymmetric imperfections on the buckling of cylindrical shells under axial compression. *Kononkl. Ned. Akad. Wetenschap. Proc. B* **66,** 265–279 (1963).
46. D. Bushnell, Stress, stability and vibration of complex, branched shells of revolution. *Comput. Struct.* **4,** 399–435 (1974).
47. PATRAN-Plus User Manual, Release 2.4, PDA Engineering, Costa Mesa, CA (1989).
48. W. D. Bushnell, F. A. Brogan, H. Cabiness and C. Rankin, STAGSPP, Lockhead Missiles and Space Co., Inc., Palo Alto, California, a postprocessor for STAGS (not released as of this writing).
49. E. Riks, Some computational aspects of the stability analysis of nonlinear structures. *Comput. Meth. appl. Mech.* **47,** 219–259 (1984).
50. G. M. Stanley, K. C. Park and H. Cabiness, The computational structural mechanics testbed structural element processor ES7: revised ANS shell elements. NASA CR 4360, NASA Langley Research Center, Hampton, VA (1991).